High-Resolution Proteomics Unveils Salivary Gland Disruption and Saliva-Hemolymph Protein Exchange in *Plasmodium*-Infected Mosquitoes

Authors: Thiago Luiz Alves e Silva[1#], Sachi Kanatani[2], Ana Beatriz Barletta Ferreira[1], Cindi Schwartz[3], Octavio A.C. Talyuli[1], Janet Olivas[1,8], Bianca M. Nagata[4], Zarna Rajeshkumar Pala[1,9], Tales Pascini[1,10], Derron A. Alves[4], Ming Zhao[5], Motoshi Suzuki[5], Lilian P. Dorner[6], Friedrich Frischknecht[6,7], Isabelle Coppens[2], Carolina Barillas-Mury[1], Jose M.C. Ribeiro[1], Photini Sinnis[2], Joel Vega-Rodriguez[1#]

[1]Laboratory of Malaria and Vector Research, National Institute of Allergy and Infectious Diseases, National Institutes of Health, Rockville, MD 20852, USA.

[2]The W. Harry Feinstone Department of Molecular Microbiology and Immunology and Johns Hopkins Malaria Research Institute, Bloomberg School of Public Health, Johns Hopkins University, Baltimore, MD, 21205, USA.

[3]Microscopy Unit, Research Technologies Branch, Rocky Mountain Laboratories, National Institute of Allergy and Infectious Diseases, National Institutes of Health, Hamilton, MT 59840, USA.

[4]Infectious Disease Pathogenesis Section, National Institute of Allergy and Infectious Diseases, National Institutes of Health, Rockville, MD 20852, USA.

[5]Research Technologies Branch, National Institute of Allergy and Infectious Diseases, National Institutes of Health, 5625 Fishers Ln, Rockville, MD, 20852, USA

[6] Integrative Parasitology, Center for Infectious Diseases, University of Heidelberg Medical School, Heidelberg, Germany

[7]German Center for Infection Research, partner site Heidelberg.

[8]Present address: Department of Pathology, New York University Grossman School of Medicine, New York, NY

[9]Present address: Biological Sciences Graduate Program, University of Maryland, College Park, MD 20742

[10]Present address: Sanaria Inc., 9800 Medical Center Drive, Rockville, MD 20850, USA.

Corresponding authors:

Joel Vega-Rodriguez: joel.vega-rodriguez@nih.gov

Thiago Luiz Alves e Silva: thiagoluiz.alvesesilva@nih.gov

Abstract:

Plasmodium sporozoites, the stage that initiates a malaria infection, must invade the mosquito salivary glands (SGs) before transmitting to a vertebrate host. However, the effects of sporozoite invasion on salivary gland physiology and saliva composition remain largely unexplored. We examined the impact of *Plasmodium* infection on *Anopheles gambiae* salivary glands using high-resolution proteomics, gene expression, and morphological analysis. The data revealed differential expression of various proteins, including the enrichment of humoral proteins in infected salivary glands originating from the hemolymph. These proteins diffused into the SGs due to structural damage caused by the sporozoites during invasion. Conversely, saliva proteins diffused out into the circulation of infected mosquitoes. Moreover, infection altered saliva protein composition, as shown by proteomes from saliva collected from mosquitoes infected by *P. berghei* or *P. falciparum*, revealing a significant reduction of immune proteins compared to uninfected mosquitoes. This reduction is likely due to the association of these proteins with the surface of sporozoites within the mosquito salivary secretory cavities. The saliva protein profiles from mosquitoes infected with both *Plasmodium* species were remarkably similar, suggesting a conserved interaction between sporozoites and salivary glands. Our results provide a foundation for understanding the molecular interactions between *Plasmodium* sporozoites and mosquito salivary glands.

Introduction

Malaria, a major mosquito-borne disease, accounted for 249 million cases and 606,000 fatalities in 2022 (1). The disease is caused by *Plasmodium* parasites and is transmitted to humans by the bite of an infected *Anopheles* mosquito. To curtail the spread of malaria, different countries have effectively adopted vector control programs by using insecticides. However, the emergence of insecticide-resistant mosquitoes has impeded elimination efforts, leading to the rebound of the disease in some countries (2). Therefore, alternative strategies to thwart parasite transmission by infected mosquitoes are needed.

The development of *Plasmodium* parasites in mosquitoes is a lengthy, complex process involving the interaction with different mosquito tissues. Infection begins when a mosquito ingests gametocytes while feeding on an infected host. Within the first hour, fertilization occurs in the mosquito midgut, and 20 hours later, ookinetes invade the midgut epithelium and differentiate into oocysts. Each oocyst undergoes sporogony, producing thousands of sporozoites. Around 9 to 12 days post-midgut invasion, sporozoites emerge from the oocyst and journey through the mosquito hemolymph to the salivary glands (SGs), which they invade (3-5). Sporozoites can reside within the SGs for the entire mosquito lifespan, entering a state of translational repression in which sporozoites are believed to decrease their metabolic activity until they are delivered into the skin of a new host when they promptly reverse the translational repression (6-8). Notably, SG sporozoites metabolize sugars and sustain active mitochondria, indicating that a basic level of metabolic activity is vital (9, 10). Much of sporozoite biology within SGs, including the mechanisms by which the sporozoite obtains nutrients to fulfill its specific metabolic requirements, remains unknown. A better understanding of

sporozoite-SG interactions can guide the development of strategies to interrupt parasite transmission.

During mosquito probing, sporozoites are delivered into the host's skin along with mosquito saliva, which contains active molecules that interfere with host hemostasis and the immune response, including complement activity, inflammation, and white blood cell responses (11). Transgenic mosquitoes lacking SGs display increased biting frequency and probing time, yet the volume of blood ingested remains unchanged, highlighting the importance of saliva in regulating feeding behavior (12, 13). Conversely, saliva proteins also influence parasite activity and, thereby, infectivity. The saliva protein mosGILT associates with the sporozoite surface, reducing sporozoite motility (14). In contrast, the saliva protein SAMSP1 binds to the sporozoite surface, increasing gliding and cell traversal activity (15). Interestingly, sporozoite infection of the SGs notably changes the saliva composition and decreases the activity of certain saliva enzymes through an unknown mechanism (16-18). Some reports highlight that mosquitoes infected with sporozoites exhibit longer probing times and a greater propensity for multiple blood feedings, indicating modified feeding behavior (16, 19-22). However, other reports found no change in the probing time between infected and uninfected mosquitoes (5, 23). These discrepancies might result from the parasite-mosquito combination used for each study or time-sensitive changes during infection of the SGs (24). Clarifying the impact of sporozoites on saliva composition is crucial for unraveling the dynamics behind host-pathogen interactions.

The SGs act as a critical bottleneck for sporozoite transmission — of the thousands of parasites that invade the SGs, only a small fraction is transmitted, making this stage an attractive target for transmission-blocking strategies. However, a comprehensive understanding of how sporozoites affect the protein composition in

the SGs remains incomplete. Previous proteome studies have been constrained by a limited number of proteins identified and by the use of total salivary gland homogenate and not saliva (17, 18). Here, we performed high-resolution proteomics of SGs from *Plasmodium berghei*-infected or uninfected *Anopheles gambiae* mosquitoes to uncover the impact of sporozoites on SG protein expression. We also investigated the impact of *P. berghei* and *Plasmodium falciparum* sporozoites on saliva composition. We found that SGs are disrupted by parasites, leading to substantial exchange of proteins with the hemolymph. Our findings not only expand the list of previously identified proteins but also offer new insights into the structural and cellular biology of the mosquito SG during sporozoite infection.

Results

The proteome of uninfected and *P. berghei-infected An. gambiae* SGs

To understand how *Plasmodium* sporozoites impact the protein composition of mosquito SGs, we performed high-resolution proteomics of uninfected and *P. berghei*-infected SGs from *An. gambiae* mosquitoes 21 days post-infection (Fig. 1 and Supplementary Fig. 1). We identified 3497 proteins comprising mosquito or parasite proteins, each containing at least three unique peptides. Hence, 2816 *An. gambiae* proteins were identified in the uninfected SGS (uSGs) (average detection of 2577.67, n=3), and 2842 proteins in *P. berghei*-infected SGs (iSGs) (average of 2647.33, n=3) (Fig. 1A and Supplementary Table 1). Additionally, we detected 277 *P. berghei* sporozoite proteins (Supplementary Table 2).

To compare the composition of different functional groups between uSGs and iSGs, we used the relative abundance of protein families (25, 26). Using SignalP 5.0 (27), we observed that proteins containing a signal peptide constituted 67% and 63% of the total protein mass in uninfected and infected samples, respectively (Fig. 1B). Functional annotation based on gene ontology revealed that the category of secreted proteins, which includes the classical saliva proteins and excludes transmembrane proteins or intra-cellular proteins, accounted for 66% of the total protein mass in uSGs and 62% of the total mass in the iSGs (Fig. 1C, D, and Supplementary Table 3). In contrast, protein synthesis, the second largest category, constituted only approximately 9% of both groups (Fig. 1C, D and Supplementary Table 3). We observed a significant increase in the relative mass of 13 functional families, where lipid transport (5 proteins) and iron transport (4 proteins) had the most salient ratio increase of three- and two-fold, respectively (Fig. 1E, F).

Plasmodium infection induces differential expression of salivary gland proteins.

Principal component analysis (PCA) revealed that uninfected and iSGs formed two distinct clusters (Fig. 2A), with PCA 1 accounting for 29% of protein variance and PCA 2 for 22%, suggesting that salivary gland invasion by *P. berghei* sporozoites impacts protein expression. A Venn diagram revealed that 31 proteins were exclusive to uSGs, 57 were exclusive to iSGs, considering proteins detected in at least two out of three replicates, whereas 2591 proteins were commonly detected in both uSGs and iSGs, considering proteins detected in at least four out of six samples including uSGs and iSGs (Fig. 2B and Supplementary Tables 4-6). Importantly, in this analysis, we considered only proteins identified with at least three unique peptides for stringency. Proteins exclusively detected in one condition were deemed differentially expressed, while commonly found proteins were separately analyzed for differential expression. A volcano plot of commonly found proteins revealed 24 upregulated proteins and seven downregulated (Fig. 2C), distributed across 13 functional classes (Fig. 2D). Remarkably, in the list of the classical saliva proteins, only three were differentially expressed: poly(U)-specific endoribonuclease (EndoU) was upregulated (Fig. 2D and Supplementary Table 7), and D7r3 and a 5’ ectonucleotidase (5’-ntd) were downregulated, (Fig. 2E). The remaining saliva proteins had a consistent, but not significant, trend for lower expression (Fig. 2E).

In the iSGs proteome, *P. berghei* infection was associated with the downregulation of two saliva proteins: D7r3 (51% reduction) and a 5'-ectonucleotidase (5'-NTD) (33% reduction) (Fig. 2D, E). Both proteins modulate hemostasis; D7r3 binds tightly to histamine, a biogenic amine that promotes itching and is an agonist for platelet activation, thus neutralizing its activity (28, 29). The 5'-NTD decreases

hemostasis by converting AMP to adenosine, an antagonist of platelet aggregation, by binding to the A2A receptor (30). Additionally, the adenosine product promotes vasodilation (31) and immunosuppression (32). Conversely, *P. berghei* infection induced a strong upregulation of the EndoU (9.8 times upregulated) (Fig. 2 D). Although the function of EndoU has not been characterized in *A. gambiae*, in *Drosophila*, EndoU plays pleiotropic roles, controlling different activities such as muscle function and lipid metabolism. EndoU specifically binds to the thoracic muscles, influencing the fly's ability to climb and preventing the accumulation of misfolded proteins within the muscle fibers (33). Moreover, EndoU regulates lipid homeostasis during aging (34). Further investigation into EndoU will help elucidate its potential function in sporozoite infection and salivary gland pathology.

Several of the differentially expressed proteins in *P. berghei* iSGs, are involved in energy metabolism (Fig 2D, E). These changes can be divided into three general processes: substrate acquisition for oxidative metabolism, mitochondrial adaptations, and iron transport. Sporozoites uptake carbohydrates for energy production and scavenger lipids that could potentially be incorporated into membranes (9, 10, 35). Furthermore, glucose has been demonstrated to support *P. berghei* viability within the iSGs (9). We found two alfa-amylases—enzymes that hydrolyze starch and glycogen into low-molecular-weight carbohydrates, like dextrin and maltose—upregulated in iSGs (AGAP012401-PA, FC = 3.8; AGAP012400-PA, detected exclusively in iSGs). These enzymes are expressed in the anterior section of the salivary glands, a region not invaded by sporozoites, and associated with sugar feeding, not blood feeding, suggesting that these enzymes could support sporozoite survival by enhancing mosquito sugar feeding thus making simpler saccharides available to the parasite (Fig. 2D and Supplementary

Table 7). Another protein related to lipid acquisition, lipophorin (AGAP001826-PA), was enriched threefold in iSGs (Fig. 2D and Supplementary Table 7). Lipophorin, the primary insect lipoprotein, circulates in the hemolymph, shuttling neutral lipids and cholesterol between different tissues. This protein is required for oocyst growth and sporogony, and in lipophorin-depleted mosquitoes, sporozoites display decreased mitochondrial activity and infectivity (10, 35). Interestingly, the functional class of lipid transport proteins (six proteins) was three times more abundant in iSGs than in uSGs (Fig. 1E and Supplementary Table 3). Immunofluorescence assays (IFA) and western blot confirmed that lipophorin levels were higher in iSGs than in uSGs, suggesting that the sporozoites may have access to an abundant supply of lipids inside the SGs (Fig. 5B and Supplementary Fig. 2).

Aligned with increased access to carbohydrates and lipids, our proteome analysis suggests increased oxidative metabolism in iSGs. The mitochondrial pyruvate carrier was upregulated in iSGs (Supplementary Table 6). This protein transports pyruvate — the end product of the glycolytic pathway— into the mitochondrial matrix for subsequent oxidation in the tricarboxylic acid cycle, thereby modulating the substrate flow to this cycle (36, 37). Additionally, in the iSGs, we observed an increase in the expression of the cytochrome C oxidase assembly protein (FC= 1.6, Supplementary Table 7), which is involved in assembling the cytochrome C oxidase complex, the final component of the mitochondrial respiratory chain (38). Cytochrome C oxidase transfers electrons from cytochrome C to oxygen, generating a proton gradient that drives ATP synthesis.

In iSGs, we observed a significant enrichment (2.3-fold increase in relative abundance) in the class of iron transport proteins —transferrin 1, ferritin light, and heavy chain— consistent with increased oxidative metabolism and cytochrome

assembly (Fig. 1E). Transferrin was 4.8 times more abundant in iSGs than uSGs (Fig. 2D), suggesting a higher demand for iron in iSGs, an essential element in various metabolic processes, such as heme biosynthesis and the electron transport chain. Alternatively, the increase in transferrin and ferritin may participate in nutritional immunity, where the host sequesters metals such as iron to deprive invading pathogens of this essential micronutrient, a phenomenon observed in *Drosophila melanogaster* (39, 40).

The extent to which SGs mount an immune response to invading sporozoites remains unknown. The prophenoloxidase pathway (PPOp) is one of the main components of the mosquito immune response, producing melanin and reactive species that are lethal to pathogens. Our data shows a strong upregulation of the PPOp proteins at three different activation steps: recognition, signal amplification, and effector response. LRIM1 is a leucine-rich protein crucial in recognizing pathogens, including *Plasmodium* ookinetes (41). LRIM1 forms a ternary complex with APL1C and TEP1 that activates the PPOp through a cascade of Clip-domain serine proteases (CLIPs) (41, 42). LRIM1 was detected exclusively in iSGs (Supplementary Table 6), whereas TEP1 showed a non-significant two-fold increase in iSGs. We identified nine CLIPs in our proteome, among which one effector and two regulatory CLIPs were differentially expressed (Fig. 2D). CLIPB4, upregulated 12-fold in iSGs, is an effector serine protease that activates the PPOp, leading to the melanization of invading ookinetes (43). Two negative regulators of PPOp were up-regulated: CLIPA14, a serine protease homolog protein (CLIP-SH), was 6.8 times more abundant, and CLIPA7 (CLIP-SH) was detected exclusively in iSGs (43, 44). Using immunohistochemistry (IHC), we detected a substantial accumulation of CLIPA14 within the iSG cavities and on the surface of sporozoites (Supplementary Fig. 3A), while the expression in the

hemolymph remained unchanged (Supplementary Fig. 3B). Phenoloxidases (POs), the main effector of the melanization pathway, are enzymes derived from Prophenoloxidases (PPOs) through the proteolytic cleavage mediated by CLIP domain serine proteases. We detected four PPOs (PPO2, PPO5, PPO6, and PPO9) in our SG proteome, in which two PPOs were differentially expressed: PPO6 was upregulated 2.4-folds in iSGs (Fig. 2D), and PPO9, known for mediating late-phase immunity against *P. berghei* oocysts, was detected solely in the uSGs (Supplementary Table 5) (45). Interestingly, we detected a strong association of PPO6 to the surface of sporozoites within the SGs (Supplementary Fig. 3C).

The initial substrate for PPOs is the amino acid tyrosine. Phenylalanine–4-hydroxylase (PAH), which hydroxylates phenylalanine to produce tyrosine (46, 47), was upregulated 2.8-fold in iSGs (Fig. 2D). Additionally, a yellow protein (AGAP003095-PA), involved in tyrosine-mediated tanning processes such as pigmentation and sclerotization, was detected exclusively in iSGs. Yellow proteins can accelerate melanization through their activity as dopachrome conversion enzymes (DCEs) (48). Interestingly, despite the upregulation of critical components of the PPOp, sporozoite melanization has never been reported within SGs. Recent findings suggest that sporozoites evade melanization in the hemolymph through post-translational modifications of cell surface proteins mediated by glutaminyl cyclase (49), indicating an evolved mechanism to evade melanization. However, glutaminyl cyclase knockout sporozoites were not melanized inside the SGs, suggesting that the SGs have an efficient mechanism to prevent melanization. It is possible that the salivary peroxidase of anophelines, an enzyme that destroys catecholamines (50-52), may inhibit the melanization response by reacting with its substrates.

We also detected a 2-fold upregulation of TEP15 in iSGs (Fig. 2D), a thioester-containing protein found in mosquito hemolymph and in male seminal fluid (53, 54). TEP15 expression is controlled by the Toll pathway, suggesting a potential role in immunity (55). We also detected strong upregulation of gelsolin in iSGs (6.8-fold increase, Fig. 2D), a key component of clotting fibers in the hemolymph of *D. melanogaster* (56).

Accumulation of upregulated proteins in the iSGs

To validate our results, we performed IFA on uSGs and iSGs. We confirmed stronger TEP15, transferrin-1, and PPO6 staining in the iSGs compared to uSGs (Fig. 3A-C). The expression of the anopheline anti-platelet protein (AAPP), a classical saliva protein expressed in the distal region of the lateral lobes, remained unchanged, corroborating our proteome data (Fig. 3D). In agreement with increased PPO levels in iSGs, we consistently observed discrete melanization spots on the surface or within the iSGs, which were prevalent in infected glands (Fig. 3E and F). Interestingly, melanization was limited to isolated spots, and widespread melanization did not occur in any iSGs, suggesting that sporozoites either inhibit the process directly or exploit a mosquito mechanism that prevents melanization in the SGs.

Protein Accumulation in iSGs Occurs Independently of Transcriptional Activity

In the iSG proteome, we observed the enrichment of proteins typically produced in mosquito tissues other than the SGs. Notable examples include lipophorin and CLIPA14, which are chiefly expressed in the fat body (57, 58); transferrin 1, highly expressed in antimicrobial hemocytes (58); and PPO6, expressed in hemocytes (58, 59). We hypothesized that these proteins could either be

synthesized in the infected iSGs or be imported from the hemolymph. To determine whether *P. berghei* infection induces the transcription of these genes in the SGs, we performed qPCR on uSGs and iSGs 20 days post-infection. As a positive control, we selected five saliva genes known to be highly expressed in the SGs: three genes that were not differentially expressed in the proteome (antigen 5, apyrase, and AAPP) and two genes that were downregulated (5' ectonucleotidase and D7r3). No significant difference in transcription was observed for these genes between uSGs and iSGs, except for AAPP and D7r3, which were strongly upregulated in iSGs (Fig. 4A). The upregulation of D7r3 transcription could be a response to the reduced protein levels upon sporozoite infection, whereas the strong upregulation of AAPP transcription is puzzling and requires further study to understand it's regulatory mechanism upon sporozoite invasion. Then, we tested the transcriptional activity of four genes known to be produced outside the SGs. In iSGs, CLIPA14 and PPO6 mRNA expression were downregulated, while transferrin and lipophorin levels remained unchanged (Fig. 4B). Note that the transcript levels for these genes are extremely low. Presumably, these mRNAs originate from other cells that remain attached to the SGs after dissection, like fat body and hemocytes.

To pinpoint whether these genes were expressed in the SGs or any tissue attached to them, we performed *in situ* hybridization of uSGs and iSGs using specific probes for lipophorin, PPO6, and apyrase. In uSGs, apyrase expression was localized to the distal portion of the central lobe and a distinct spot in the anterior region of the lateral lobes (Fig. 4C and Supplementary Fig.4). In iSGs, apyrase showed a similar pattern, except in the anterior region of the lateral lobes, which exhibited strong transcriptional activity. This suggests that SG infection can alter the transcriptional pattern of saliva proteins, which are traditionally believed to be

restricted to specific SG sites. In both conditions, lipophorin expression was confined to the fat body cells associated with the SGs, whereas PPO6 was detected in hemocytes attached to iSGs (Fig. 4C). These results support that lipophorin, PPO6, and presumably other humoral proteins enriched in iSGs, originate from external tissues. Henceforth, we will refer to these proteins as enriched or depleted instead of up or downregulated.

Sporozoite invasion compromises the SG epithelial integrity

In the *P. berghei iSG* proteome, many enriched proteins matched those circulating in high concentrations in the hemolymph (62). Since it is unlikely that SGs produce some of these proteins (e.g., lipophorin and PPO6), we hypothesized that hemolymph proteins might enter the SGs due to structural damage inflicted by sporozoites during salivary gland invasion (22). Consequently, we also expected to find saliva proteins in the hemolymph of infected mosquitoes. To gain insight into the hemolymph composition of infected mosquitoes, we performed high-resolution proteomics on *A. gambiae* hemolymph 19 days post-infection, when many sporozoites had invaded the SGs (Supplementary Tables 8). This analysis confirmed that several proteins abundantly present in the infected hemolymph coincided with those enriched in the iSGs (Fig. 5A, Supplementary Fig. 5A, B, and Supplementary Tables 6 and 7). Notably, we detected abundant saliva proteins, such as apyrase and antigen 5, among those found exclusively in the *P. berghei*-infected hemolymph (Supplementary Fig. 5C, Supplementary Table 8). Western blot analysis using antibodies against lipophorin (a hemolymph marker) and apyrase (a saliva marker) confirmed that lipophorin was enriched in the iSGs but not in the uSGs (Fig. 5B). In contrast, apyrase was detected in the hemolymph of

infected mosquitoes 21 days post-infection but not at 9 days post-infection when the SGs had not yet been invaded (Fig. 5C).

To investigate whether sporozoite invasion compromised the epithelial integrity of iSGs, we measured the diffusion of fluorescent dextran from the hemolymph into the SGs after intrathoracic injection in uninfected and infected mosquitoes 21 days post-infection. We found that 90% of the iSGs showed dextran invasion, compared to only 10% of the uSGs (Fig. 5D). These results confirm that sporozoite-induced epithelial disruption facilitates the bidirectional exchange of proteins between the hemolymph and saliva, explaining the presence of proteins not produced in the SGs. Importantly, these findings are consistent with a previous report that found damage to salivary glands during sporozoite invasion (60)

Next, we performed transmission electron microscopy (TEM) to observe the effect of sporozoite infection on saliva. In TEM images, the saliva appears as a dense, homogeneous matrix inside the secretory cavities (63). Interestingly, in iSGs, the saliva often became granular with electron-lucent spaces, likely due to the leakage of saliva proteins outside the secretory cavities (Fig. 5F). This phenomenon was confirmed by two additional laboratories in *A. stephensi* SGs infected with *P. berghei* (Supplementary Fig. 6). Further studies are needed to assess the nature of these morphological changes in saliva and their impact on parasite development and transmission.

Increased interaction of hemocytes with iSGs

The interaction of hemocytes with SGs in uninfected and infected mosquitoes has not been documented. However, we observed instances of PPO6-positive hemocytes adhering to the surface of SGs (Fig. 4C). Interestingly, when performing the dextran diffusion assay, we found hemocytes that had taken up

dextran attached to the surface of iSGs (Fig. 5G, H, and Supplementary Fig. 7). Quantification revealed that iSGs had significantly more attached hemocytes containing dextran than uSGs (Fig. 5H). Importantly, the number of hemocytes attached to iSGs may be underestimated due to limited visual contrast, which complicates the differentiation of hemocytes from adjacent tissues in areas of strong dextran invasion. The increased presence of hemocytes on iSGs likely impacts the detection of proteins on the iSGs proteome. Further studies are required to elucidate the role and molecular profile of these hemocytes.

Sporozoite-induced changes in the composition of saliva proteins

Mosquito saliva plays a major role in blood feeding and the dynamics of sporozoite transmission (61). To assess how *Plasmodium* infection and associated salivary gland damage affect saliva composition, we performed label-free quantitative proteomics on saliva samples from uninfected and infected mosquitoes 21 days post-feeding. We performed separate comparative analyses for *P. berghei* and *P. falciparum* infections. Saliva was harvested by inserting the mosquito proboscis into micropipette tips containing 2% pilocarpine, an inducer of salivation, in PBS (Supplementary Fig. 8A). Infected mosquitoes contained between 15,000 and 80,000 sporozoites in their SGs, with a median of 45,000 sporozoites per mosquito (Supplementary Fig. 8B). We identified an average of 85 proteins in the saliva of uninfected *An. gambiae* mosquitoes and 41 in *P. berghei*-infected mosquitoes. Similarly, we identified an average of 106 proteins in uninfected saliva and 69 in *P. falciparum*-infected saliva, with each sample containing at least three unique peptides in at least one group (Fig. 6A, B, and Supplementary Tables 9 and 10). Functional analysis, based on relative protein abundance, revealed that 63 to 73%

of proteins in uninfected saliva possessed signal peptides, compared to 58% in *P. berghei*-infected saliva and 75% in *P. falciparum*-infected saliva (Fig. 6C, D). Gene ontology analysis revealed that secretory proteins, which include classical saliva proteins typically found in the hematophagous insect sialomes, were the most prevalent category in all groups (Fig. 6E, Supplementary Table 11).

To understand how SG infection impacts saliva composition, we performed PCA on uninfected and infected saliva. This analysis revealed two distinct protein clusters, clearly separating infected from uninfected saliva for both *P. berghei* and *P. falciparum* (Fig. 6F, G). For experiments with *P. berghei*, 26 proteins were exclusively found in the uninfected saliva, whereas 65 proteins were common to both groups. For experiments with *P. falciparum*, 25 proteins were unique to uninfected saliva, and 87 were found in both replicates (Fig. 6H and Supplementary Tables 9 and 10). Proteins were classified as differentially enriched or depleted if exclusively detected in one condition or showed statistically significant differences in expression between conditions. Among proteins common to both conditions, 22 depleted proteins for *P. berghei*-infected saliva (Fig. 7A and Supplementary Table 12), and 43 were depleted in *P. falciparum*-infected saliva (Fig. 7B and Supplementary Table 13). Interestingly, a strong trend of protein depletion was observed, with no proteins enriched in saliva from iSGs. Analysis of the differentially enriched or depleted proteins revealed a notable trend: several hemolymph proteins that were enriched in the SGs following sporozoite invasion exhibited depletion in the saliva collected from infected mosquitoes (Figs. 2D, and 7C, D, and Supplementary Tables 7, 12, 13). This pattern was particularly evident in immune proteins such as PPO6, TEP15, and CLIPA14.

Among the classical saliva proteins identified, three were depleted in *P. berghei*-infected saliva, while twelve were depleted in *P. falciparum*-infected saliva (Fig.

7E, F, and Supplementary Tables 12-13). The depletion of these proteins may facilitate sporozoite transmission by prolonging probing time and increasing the biting rate of infected mosquitoes. Further studies are needed to ascertain the effects of differential expression of these salivary proteins on blood feeding and pathogen transmission. Additionally, even among proteins that were not significantly depleted, a general trend toward decreased protein level was observed (Fig. 7E, F). This combined decrease in protein levels may affect blood feeding, leading to longer probing times and more bites required for successful feeding, thereby increasing the probability of sporozoite inoculation and transmission.

Humoral proteins attach to the surface of sporozoites

Most sporozoites that invade the SGs remain within this tissue throughout the mosquito lifespan and are never injected into a new host. The attachment of specific hemolymph proteins enriched in the whole SG proteome, such as PPO6 and CLIPA14, to the sporozoite surface (Fig. S3A, 3C) could potentially explain the depletion of these proteins in the saliva proteome: their binding to the sporozoite could reduce their presence in the saliva. To confirm this, we used immunohistochemistry and immuno-transmission electron microscopy. We selected three hemolymph proteins enriched in the whole SG proteome but depleted in the saliva proteome — TEP15, PPO6, and transferrin, for immunofluorescence analysis. Additionally, we examined AAPP, a saliva protein with consistent detection in both uSGs and iSGS proteomes (Fig. 2D). Our analysis revealed that TEP15, PPO6, and transferrin were closely associated with the sporozoite surface of the sporozoites. In contrast, AAPP was dispersed throughout the SGs cavities rather than located on the parasite surface (Fig. 8 and

Supplementary Fig. 9). This pattern supports the hypothesis that proteins adhering to the sporozoite surface within the SGs are less likely to be inoculated with the saliva.

Discussion

The sporozoite colonization of mosquito SGs is a critical yet often overlooked phase of the malaria parasite's lifecycle. This stage represents a bottleneck for sporozoite transmission and, thus, offers a promising target for malaria prevention. However, fundamental questions remain regarding how SGs respond to sporozoite invasion and how sporozoites survive within SGs for extended periods. Our research reveals that sporozoite invasion induces morpho-physiological changes in the gland, altering the composition of saliva proteins and potentially influencing malaria transmission. Notably, both *P. berghei* and *P. falciparum* infections triggered similar changes in the saliva proteome, reinforcing the role of *P. berghei* as a robust model for studying sporozoite-SG interactions. Additionally, while earlier transcriptome studies cataloged the genes expressed in *An. gambiae* SGs, earlier proteomic analyses using 2D gels lagged, identifying only 69 to 122 unique proteins (17, 62). In contrast, using high-resolution proteomics, we significantly expanded this catalog to 3,497 mosquito and 277 parasite proteins, providing new insights into *Anopheles*-parasite interactions.

Our results reveal significant changes in key biochemical pathways, including energy metabolism and nutrient acquisition. The upregulation of proteins essential for mitochondrial respiration, such as the mitochondrial pyruvate carrier and cytochrome C oxidase assembly protein, is particularly intriguing considering earlier transmission electron microscopy studies of iSGs, which reported cellular

reorganization, with intracellular sporozoites often surrounded by mitochondria (3). These findings suggest that sporozoites may interact with or exploit critical mitochondrial pathways. The increased metabolic demand observed in salivary gland cells could be a response to mitigate damage caused by the invasion of numerous sporozoites.

We found that sporozoites that reach the secretory cavities may have access to proteins that transport essential nutrient, including lipophorin and transferrin. In mosquitoes, *Plasmodium* oocysts and sporozoites interact with lipophorin, an important lipid source for the parasite (10, 35). Lipophorin knockdown reduces oocyst numbers and size and produces less infectious sporozoites (10). Interestingly, *Plasmodium* oocyts seem to modulate lipid metabolism in mosquitoes by releasing an unknown factor that increases lipophorin expression (63). Another nutrient that sporozoites may access is iron. Transferrin, a glycoprotein that shuttles iron among different tissues, was observed binding to the sporozoite surface within the SGs. Moreover, in other models, transcription of transferrin increases after mosquito infection, suggesting a potential role in the immune response (64). In *Drosophila*, transferrin participates in nutritional immunity by sequestering iron, thereby hindering pathogen access to this micronutrient (40). Further studies are needed to determine whether sporozoites exploit host nutrients during the salivary gland stage.

Previous transcriptome studies reported the upregulation of immune genes in the iSGs, implying that the SGs are immunocompetent (9). A limitation, however, was the absence of biological evidence confirming the origin of these mRNAs. This is important, as SGs may be contaminated with other tissues during dissection, such as fat bodies and hemocytes, which respond to infection. The fact that the hemolymph immune proteins upregulated in the proteome of iSGs were not

upregulated in the RT-qPCR and *in situ* hybridization analysis suggests that these proteins most likely entered the SGs due to structural damage to the epithelial layer, as observed in our dextran diffusion assay and previously reported (24, 60). However, we cannot exclude the possibility that iSGs may import some of these proteins via a specific, yet unidentified, mechanism (pinocytosis or receptor-mediated transcytosis). Moreover, we found that hemocytes are attracted to the iSGs, potentially contributing to the detection of immune proteins in our proteomic analysis. Though novel, this finding is unsurprising, as mosquito hemocytes patrol epithelial tissues searching for pathogens (65). Furthermore, these immune cells may contribute to tissue regeneration, as observed in *Drosophila* and mammals, specifically M2 macrophages (66, 67).

Our findings suggest that sporozoites within the salivary gland are closely associated with hemolymph proteins, especially those from the phenol-oxidase pathway. This association raises the question of how the sporozoites evade melanization within the SGs. A known evasion mechanism for hemolymph sporozoites involves post-translational modifications of cell surface proteins by the parasite's glutaminyl cyclase (49). However, this mechanism does not account for sporozoites in the SGs, as knockout parasites within the SGs were not melanized, supporting the idea that the SGs are an immunoprivileged tissue (49). Another possibility is that the parasite recruits factors that inhibit melanization. In iSGs, we detected an enrichment of CLIPA14, which was bound to the parasite surface. CLIPA14 acts as an agonist for *Plasmodium*, inhibiting the PPO pathway (68, 69). Thus, the parasite may recruit negative regulators to prevent PPO activation.

Saliva proteins are crucial to vectorial capacity, influencing blood feeding, oocyst development, and sporozoite transmission (61, 70, 71). Therefore, we investigated whether changes in the salivary gland proteome affect saliva composition.

Surprisingly, we found that the humoral hemolymph proteins enriched in iSGs were depleted in the saliva of *P. berghei* and *P. falciparum*-infected mosquitoes, with many being immune proteins adhering to the parasite inside the glands. Notably, for both parasites, we observed a reduction in yellow proteins and EndoU and, for *P. falciparum*, a decrease in one D7 protein. All other saliva proteins tended toward depletion. This collective decrease in saliva proteins may alter parasite transmission dynamics, potentially increasing probing time and bite frequency, thereby favoring sporozoite transmission (16, 22).

We observed that salivary gland invasion by sporozoites causes epithelial damage, resulting in the leakage of saliva proteins into the mosquito hemolymph. This leakage can potentially impact mosquito physiology, as some of these proteins include enzymes, protein inhibitors, and kratagonists (proteins that sequester signaling molecules), which could disrupt basic signaling pathways. Previous studies show that sporozoites cause minimal damage to invaded SG cells by utilizing the AMA1-RON complex to form a vacuole with a ring-like structure that mimics a moving junction (24, 60). This is essential to maintain the general structure of the SG by preventing the rapid loss of salivary gland cells and the collapse of the SG. However, our results show that although sporozoites do not induce the massive loss of SG cells, the invasion disrupts the structural integrity of the tissue, leading to saliva leakage, as previously suggested (24). The implications of saliva proteins entering the mosquito hemolymph, particularly concerning to parasite development, merit further investigation.

Overall, our results provide an updated catalog of protein expression in *A. gambiae* SGs. We found that complex dynamic processes — transcriptional activity, epithelial damage, and hemocyte attraction— influence changes in protein abundance in this tissue. Collectively, these elements may affect mosquito feeding

behavior and, consequently, sporozoite transmission. This study offers a functional description of sporozoite salivary gland interactions, setting the stage for future studies focused on the consequences of epithelial damage on parasite transmission, the nutritional requirements of parasites, the impact of saliva proteins on the mosquito hemocoel, and the influence of hemocytes in the infection process. These will open avenues for understanding the salivary gland bottleneck and preventing transmission of sporozoite.

Material and Methods

Parasites, mosquitoes, and infections

Anopheles gambiae Keele strain (72) was reared at 28 °C and 80% relative humidity, with a 12 h/12 h light/dark cycle under standard laboratory conditions. Adult mosquitoes were fed *ad libitum* at 10% sucrose solution.

Plasmodium berghei infection

For the proteome, we performed infections with a transgenic GFP *P. berghei* parasite strain (ANKA GFPcon 259cl2). For all the other assays, we used *P. berghei* (Pb) ANKA transgenic line expressing mCherry and luciferase markers under the control of the hsp70 and eef1a promotors, respectively (73). Parasitemia was quantitatively assessed by light microscopy using methanol-fixed, 10% Giemsa-stained blood smears. For mosquito infections, female mosquitoes (4-5 days old) were fed on infected mice once flagellation reached 3-4 ex flagellations per 40 x field. After feeding, infected mosquitoes were kept at 19°C, 80% humidity, and a 12-hour light-dark cycle. Mosquitoes with a productive infection in the salivary glands were sorted using a fluorescent scope (Leica M205 FCA coupled to a camera DFC 7000 G5 for multi-color fluorescence imaging). As infection controls, mosquitoes from the same cohort were blood-fed on uninfected mice at the same time as the infected group.

Plasmodium falciparum infection

Female *An. gambiae* mosquitoes were infected with *P. falciparum* NF54 via membrane feeding using reconstituted human blood (74). The asexual blood-stage cultures were maintained in vitro using O+ erythrocytes at a 4% hematocrit, as previously described (74). For mosquito infections, a suspension of human RBCs

was mixed with human serum (Interstate blood bank) at 50% hematocrit and diluted to 0.05% gametocytemia before being fed to the mosquitoes. Post-infection, the mosquitoes were kept at 25°C and 80% humidity and provided with a 10% (w/v) sucrose solution.

Salivary gland dissection and Saliva collection

For proteomic analysis of mosquito salivary glands, we used mosquitoes infected with *P. berghei* parasite as described above. Three independent infections were conducted for the proteome analysis, each one consisting of three pools of 25 pairs of uninfected or infected salivary glands. Salivary glands were dissected 21 days post-infection and immediately added to RIPA buffer (Thermo Fisher) containing Halt™ Protease and Phosphatase Inhibitor Cocktail (Thermo Fisher). After dissection, the SGs were immediately snap-frozen in liquid nitrogen and stored at -80°C until further use.

For saliva collection, forced salivation was used on 50 female mosquitoes. Three independent infections with *P. berghei* or four with *P. falciparum* were performed for this assay; either of these parasites was paired with an uninfected sample. The mosquitoes were water-deprived for approximately 1–2 hours before collection. After sedation on ice, the mosquitoes' mouthparts were inserted into 10 µl tips containing 8 µl of PBS supplemented with 2% pilocarpine (Sigma-Aldrich). The mosquitoes were then allowed to salivate for 30 minutes at 28°C. The saliva solutions were subsequently pooled into Protein Lo-Bind tubes (Eppendorf) and stored at -80°C until further use.

Hemolymph collection

In two independent experiments, Hemolymph was collected by perfusion from 25 uninfected or *P. berghei*-infected mosquitoes. Mosquitoes were anesthetized on ice and placed individually under a stereoscope on parafilm. An incision was made on the lateral region of the VI-VII abdominal segments using a U-100 insulin syringe. A heat-stretched capillary needle filled with sterile PBS was inserted laterally into the thorax, and approximately 10 µL of sterile PBS was injected to displace the hemolymph. The hemolymph flowed through the abdominal incision and was collected with a pipette (P20, Gilson) into pre-chilled Protein LoBind tubes (Eppendorf) on ice. After collection, a protease inhibitor (Halt™ Protease and Phosphatase Inhibitor Cocktail, Thermo Fisher) was added to a final concentration of 1×.

For proteomic analysis, hemolymph samples were centrifuged at 1,000g for 10 minutes at 4°C. The supernatant (plasma) was transferred to a new Protein LoBind tube, and the pellet was discarded. The plasma was further centrifuged at 10,000g for 10 minutes at 4°C to remove prohemocytes and residual cellular debris. The clarified plasma was stored at -80°C for mass spectrometry.

Mass Spectrometry:

The samples dissolved in SDS-PAGE sample buffer were run on an SDS-PAGE minigel. The gels were stained with Coomassie blue (ProtoBlue Safe, National Diagnostics) overnight. The samples for the whole salivary gland proteome and hemolymph proteome were cut in six slices, whereas for the saliva samples, the top gel slices were excised and cut in two pieces. Next, the excised slices were cut into small pieces, and subjected to in-gel trypsin digestion. Briefly, the gel pieces were destained with 50% acetonitrile in 100mM AMBI, reduced with 5mM DTT, and

alkylated in 11mM iodoacetamide. The pieces were then dehydrated with 50%, followed by 100%, acetonitrile. Afterward, 10 ng/µL mass-spec-grade trypsin (Promega) was added, allowing the trypsin solution to soak into the gel. Following overnight digestion at 30°C, the peptides were extracted with acetonitrile in formic acid and subjected to LC-MS/MS analysis.

LC-MS/MS data were acquired using an Orbitrap Fusion Lumos mass spectrometer equipped with an EASY-Spray Ion Source and an EASY-nLC 1200 liquid chromatography system (Thermo Fisher Scientific). The mobile phase consisted of water with 0.1% formic acid. Peptides (5 µL) were loaded onto a trap column (PepMap 100 C18, 3 µm particle size, 2 cm length, 75 µm inner diameter, Thermo Fisher Scientific), and separated on an analytical column (PepMap 100 C18, 2 µm particle size, 25 cm length, 75 µm inner diameter, Thermo Fisher Scientific) using a linear gradient: 0–40% acetonitrile over 80–100 minutes, 40–80% for 5 minutes, holding at 80% for 5 minutes, 80–0% for 5 minutes, and holding at 0% for 5 min. Throughout this 120-min data acquisition, the flow rate was set at 300 nL/min, with the analytical column maintained at 50 °C.

Data acquisition followed a standard data-dependent acquisition strategy. MS1 scans were performed every 2 seconds using the Orbitrap mass analyzer at a resolution of 120,000. MS2 scans were performed on multiply charged precursor ions, isolated with a 1.6 m/z window using a quadrupole, and fragmented by CID at 35% collision energy, analyzed with the Linear Ion Trap. A dynamic exclusion period of 30 seconds was applied, and EASY-IC internal calibration was used for Orbitrap scans.

Data processing:

LC-MS/MS data were processed using MaxQuant software (v2.0.3.0.) (24). Raw data files from each sample were loaded as fractions and searched against the *Anopheles gambiae* PEST annotated protein database (VectorBase, release 51 for saliva proteome; release 54 for the whole salivary gland proteome, release 68 for the hemolymph proteome) and *Plasmodium berghei* ANKA protein database (PlasmoDB, release 51 for saliva proteome; release 54 for the whole salivary gland proteome, release 68 for the hemolymph proteome), with the MaxQuant contaminants database included. For *Plasmodium falciparum* samples, the *P. falciparum* NF54 protein database (release 51) was used. Peptide identification allowed for fixed cysteine carbamidomethylation and variable modifications of N-terminal acetylation and methionine oxidation. A 1% false discovery rate (FDR) was applied, and the *match between runs* feature was enabled. Protein quantification was performed using iBAQ intensity to generate LFQ intensity, which was reported as log2 values in tables and figures. Only proteins with at least three unique peptides were included, and contaminants were excluded from further analysis.

Statistical analyses were performed using Perseus software (75). Protein intensities were log2-transformed and normalized by median centering. Only proteins with LFQ values greater than zero were included in the analysis. Missing values were imputed using a random normal distribution, with the mean set to the observed distribution mean minus 1.8 standard deviations and the standard deviation set to 0.3 times the observed standard deviation. Differential expression was assessed using Student's t-test with permutation-based FDR control—proteins with q value ≤ 0.05 were considered differentially expressed. Heatmaps were generated on Perseus, and PCA plots were generated using GraphPad.

Protein annotation:

For protein annotation, we employed an in-house program that analyzes BLASTp and rpsBLAST results across various databases, including UniProtKB, Conserved Domain Database (CDD), REFSEQ-Invertebrate, Diptera, and FlyBase. This program evaluates approximately 400 keywords and their order of appearance in the protein matches, considering e-values and sequence coverage. Signal peptides were predicted using SignalP 5.0. Protein abundance was quantified using intensity-based absolute quantification (iBAQ). Relative abundances within each pool were calculated by dividing individual iBAQ values by the total sum of iBAQ values for that pool (25, 26, 76).

Immunofluorescence assays from whole tissue mounting

SGs were dissected from adult female mosquitoes, either uninfected or infected with *P. berghei*, 21 days post-infection. To facilitate handling, SGs were initially kept attached to the mosquito heads and detached just before mounting. The SGs were fixed in 4% paraformaldehyde at room temperature for 1 hour. Following fixation, the SGs were washed three times with PBST (PBS containing 0.1% Triton X-100) to remove residual fixative. Blocking was performed by incubating the SGs in PBST supplemented with 5% BSA (bovine serum albumin) for 1 hour at room temperature. Primary antibodies were diluted in the blocking buffer as follows: anti-TEP15 rabbit polyclonal serum (1:200, Pacific Immunology), anti-Transferrin 1 rabbit polyclonal serum (1:500, Pacific Immunology), anti-PPO6 rabbit polyclonal serum (1:500) — kindly provided by Dr. Ryan Smith from Iowa State University —, anti-AAPP rabbit polyclonal serum (1:200, Pacific Immunology), and anti-circumsporozoite (CS) protein mouse monoclonal antibody (3D11, 1:1000). SGs were incubated with these primary antibodies overnight at 4

°C. After primary antibody incubation, SGs were washed three times with the blocking buffer for 20 minutes each. They were then incubated with secondary antibodies, diluted in the blocking buffer, for 4 hours at room temperature. The secondary antibodies used were Alexa Fluor 488-conjugated, Alexa Fluor 594-conjugated goat anti-mouse or goat anti-rabbit antibodies (1:1000, Thermo Fisher). Wheat Germ Agglutinin (WGA) conjugated to Alexa Fluor 647 (Thermo Fisher) at 2 µg/ml was employed to visualize N-acetyl glucosamine residues. Following, the SGs were washed three times in PBST. They were counterstained with Hoechst 33342 (20 µM, Thermo Fisher) for 20 minutes. The tissues were mounted using ProLong Gold Antifade (Thermo Fisher). Confocal images were obtained using a Leica TCS SP8 DM8000 confocal microscope (Leica Microsystems, Wetzlar, Germany) with a 40× or 63× oil immersion objective. The microscope was equipped with a photomultiplier tube/hybrid detector. Microscope slides were mounted using a drop of Prolong Gold Antifade Mountant (ThermoFisher).

Histopathology and Immunofluorescence

Specimens were fixed in 10% neutral buffered formalin for 1hours then transferred to 70% ethanol prior to suspension in Tissue Guard Gel (TG12, StatLab) according to manufacturer's recommendations. The gel pellet was trimmed then processed in paraffin with an expedited tissue processing protocol on the Leica ASP6025. Samples were embedded into paraffin blocks then sectioned at 4-5 µm.

Staining was achieved on the Bond RX automated system with the Bond Research Detection Kit (DS9455, Leica). Tissue sections were deparaffinized with the Bond Dewaxing Solution (AR9222, Leica) at 72o C for 30 min then subsequently rehydrated with graded alcohol washes and 1x Bond Wash Solution (Leica). Heat-

induced epitope retrieval (HIER) was performed using Epitope Retrieval Solution 1 (Leica), heated to 100o C for 20 minutes. Tissues were blocked with Protein Blocker (X0909, Dako) for 30 min prior to a 60 min incubation with the following primary antibodies: anti-TEP15 rabbit polyclonal serum (1:200, Pacific Immunology), anti-Transferrin 1 rabbit polyclonal serum (1:500, Pacific Immunology), anti-PPO6 rabbit polyclonal serum (1:500) — kindly provided by Dr. Ryan Smith from Iowa State University —, anti-AAPP rabbit polyclonal serum (1:200, Pacific Immunology), anti-Lipophorin (1:400, Pacific Immunology), anti-CLIPA14 (1:400, Boster Bio), and anti-circumsporozoite (CS) protein mouse monoclonal antibody (3D11, 1:1000, Pacific Immunology). . Samples were rinsed with wash solution then incubated for 30 min with the following secondary antibody which also contained The secondary antibodies used were Alexa Fluor 488-conjugated, Alexa Fluor 594-conjugated goat anti-mouse or goat anti-rabbit antibodies (1:1000, Thermo Fisher). Wheat Germ Agglutinin (WGA) conjugated to Alexa Fluor 647 (Thermo Fisher) at 2 µg/ml. Slides were counterstained with Hoechst 33342 (20 µM, Thermo Fisher) for 20 minutes. All antibodies were diluted in Background Reducing Antibody Diluent (S3022, Agilent). Slides were mounted with ProLong Gold Antifade Mountant (P36934, Invitrogen).

Transmission electron microscopy and immune staining

Protocol at NIAID: Salivary glands were fixed in 2% paraformaldehyde in 0.1 M cacodylate buffer and stored at 4ºC until further processing. Samples were spun into a pellet for microwave assisted (BioWave, Ted Pella) electron microscopy preparation. Briefly, pellets were rinsed with buffer, dehydrated using a graduated ethanol series, and infiltrated with LR White (Electron Microscopy Sciences). Blocks were polymerized at 50ºC in a vacuum oven overnight. For immune gold labeling: 70 nm sections were placed onto carbon coated 200 hex mesh gold grids.

Sections were blocked for 1.5 hours at room temperature in 5% BSA, 10% NGS, 1% fish gelatin, and 0.01% Tween-20 in PBS. Sections were placed in primary antibody (1:50 for PP06, TEP15, and TR1) O/N at 4ºC along with a no-primary control (block only). Sections were rinsed with blocking buffer and placed in 1:20 25 nm-goat-anti-rabbit (BBI Solutions, Ted Pella) secondary antibodies for 2 hours at room temperature. Sections were rinsed with PBS, followed by dH20, and post-stained with 2% aqueous uranyl acetate. Sections were imaged with a Tecnai T12 transmission electron microscope (Thermo Fisher) operating at 120 eV with a Rio digital camera (Gatan).

Protocol at Heidelberg University: salivary glands from uninfected or *P. berghei*-infected *An. stephensi* mosquitoes were dissected on day 19 post infection and immediately fixed using 4% paraformaldehyde and 1% glutaraldehyde in 0.1 M PHEM buffer (60 mM PIPES, 10 mM EGTA, 25 mM HEPES, 2 mM Magnesium sulfate, pH 6.9) over night at 4°C. Next, using a BioWave Pro+ microwave the glands were further fixed with 1% osmium tetroxide in 0.1 M PHEM buffer and post-fixed in 1% uranyl acetate in ddH_2O. The fixed glands were dehydrated in an acetone series and embedded in Spurr's resin set to polymerize at 60 °C for 48h. Once polymerized, the block was sectioned on a Leica EM UC7 using a DiATOME diamond knife to generate 70 nm sections, which were picked up on formvar coated grids. Salivary gland sections were imaged on a 70 kV Jeol JEM1400 TEM equipped with a TVIPS TemCam F416 4k x 4k pixel digital camera.

Protocol at Johns Hopkins University: For thin-section transmission electron microscopy (TEM), salivary glands of *An. stephensi* mosquitoes containing P. *berghei* sporozoites (ANKA-strain 2.34) were fixed in 2.5% glutaraldehyde (Electron Microscopy Sciences; EMS) in 0.1 M sodium cacodylate buffer (pH 7.4)

for 1 h at room temperature. They were washed 3 times in 0.1 M cacodylate buffer and then postfixed for 1 h in 1% osmium tetroxide (EMS) in the same buffer at room temperature. After 3 washes in water the samples were stained for 1 h at room temperature in 2% uranyl acetate (EMS), then washed again in water and dehydrated in a graded series of ethanol. The samples were then embedded in Embed-812 epoxy resin (EMS). Ultrathin (50–60 nm) sections were cut using a Reichert Ultracut ultramicrotome and collected on formvar- and carbon-coated nickel grids, stained with 2% uranyl acetate and lead citrate before examination with a Philips 410 Electron Microscope (Eindhoven, the Netherlands) under 80 kV.

Dextran diffusion and detection of phenoloxidase activity

Uninfected or *P. berghei*-infected mosquitoes, 21 days post-infection, were cold-anesthetized and injected with 50 nl of 10 kDa anionic fixable dextran conjugated with Alexa Fluor 488 (1 µg/µl, Thermo Fisher). After injection, mosquitoes were maintained at 26 °C for 3 hours to allow the dextran to circulate in the hemolymph. SGs were dissected from the injected mosquitoes and fixed in 4% paraformaldehyde for 1 hour at room temperature in nine-well excavated glasses. The SGs were then washed twice with PBS to remove residual fixative and counterstained with Wheat Germ Agglutinin (WGA) 647 (2 µg/ml, Thermo Fisher) and Hoechst 33342 (20 µM, Thermo Fisher) for 30 minutes. Finally, the samples were mounted with ProLong Gold Antifade Mountant (Thermo Fisher) for imaging. To detect phenoloxidase activity, the prevalence of melanization spots was computed from two independent experiments.

Hemocyte staining

Uninfected mosquitoes were cold-anesthetized and injected with 50 nl of 10 kDa anionic fixable dextran conjugated with Alexa Fluor 488 (1 µg/µl, Thermo Fisher).

After injection, mosquitoes were maintained at 26 °C for 3 hours. The hemolymph of 15 mosquitoes (2 µl per mosquito) was collected by perfusing the mosquito abdomen with anticoagulant buffer (60% Schneider medium, 10% fetal bovine serum, and 30% citrate buffer, pH7) and immediately transferred to a well from a ibidi µ-Slide 15 Well Glass Bottom slide. The cells were allowed to adhere for 15 minutes at room temperature, and the well was washed with 2% BSA solution in PBS before being fixed in 4% paraformaldehyde for 1 hour at room temperature. The well was washed with PBS to remove the fixative solution and incubated for 20 min with 1:40 phalloidin Alexa Fluor 546 (1U, Thermo Fisher) and Hoechst 33342 (20 µM, Thermo Fisher) diluted in PBS. The incubation media was removed, the well washed with PBS, and a drop of ProLong Gold Antifade Mountant (Thermo Fisher) was added.

In situ Hybridization

Salivary glands (SGs) were dissected in PBS from uninfected or P. berghei-infected mosquitoes 21 days post-infection and immediately fixed in 4% paraformaldehyde for 1 hour at room temperature. If tissues were not processed immediately, they were stored at 4°C in paraformaldehyde until processing. We used the RNAscope™ Multiplex Fluorescent Assay (RNAscope Multiplex Fluorescent Reagent – ref# 323100 and RNAscope 4-plex Ancillary kit for multiplex fluorescent V2 – ref# 323120, Advanced Cell Diagnostics), employing three different spectral channels simultaneously. Briefly, SGs were washed with PBS to remove the fixative, then treated with 40 µL of protease IV (1 drop) at room temperature for 30 minutes to permeabilize the tissues. After two PBS washes (2 minutes each), SGs (10 pairs) were incubated with a probe mixture

diluted 1:50. The following probes were used: Apyrase (Aga – AGAP011026 – C1, cat# 1302811-C1), PPO6 (Aga – PPO6 – C2, cat# 458541-C2), and Lipophorin (Aga – AGAP001826 – C3, cat# 484941-C3). SGs were incubated with the probe mixture for 2 hours with gentle shaking at 40°C, then placed in 1 mL of 5x SSC and left overnight at room temperature. The next day, we developed the fluorescent signals for each probe following the manufacturer's instructions. For SG incubations (AMPs, HRP, and HRP blocker), 40 µL (1 drop) of reagent was used, and washes were performed with 1 mL of wash buffer (provided by the kit). The fluorescent signals were developed using Opal fluorophores (cat# NEL861001KT, Akoya Biosciences) as follows: C1 with Opal 520, C2 with Opal 570, C3 with Opal 620, and C4 with Opal 690. After the C4 signal was developed, tissues were counterstained with Hoechst (2 µM, Thermo Fisher) and Wheat Germ Agglutinin Alexa Fluor Plus 770 (2 µg/mL, Thermo Fisher) diluted in PBS for 20 minutes at room temperature. Finally, SGs were briefly rinsed with PBS and mounted with ProLong™ Gold Antifade Mountant (Thermo Fisher).

Western blot

SGs were dissected from uninfected, or *P. berghei*-infected mosquitoes 21 days post-infection and immediately placed in RIPA buffer (Thermo Fisher). A total of 10 pairs of SGs were then mixed with LDS sample buffer (Thermo Fisher) containing 5% β-mercaptoethanol (Sigma-Aldrich). Proteins were resolved on a NuPAGE™ 10% Bis-Tris Protein Gel (Invitrogen) under reducing conditions and transferred to a PVDF membrane using Invitrogen™ Power Blotter Select Transfer Stacks (Invitrogen). The membrane was blocked overnight at 4°C with 5% milk powder in TBST (Tris-buffered saline with 0.1% Tween 20). For immunoblotting, membranes were incubated with primary antibodies: rabbit anti-lipoprotein (1:500) and mouse anti-Tubulin (1:1000, Thermo Fisher), diluted in TBST for 1 hour at

room temperature. After washing three times with TBST, membranes were incubated with horseradish peroxidase-conjugated goat anti-mouse and goat anti-rabbit secondary antibodies (1:30,000 in TBST, Sigma-Aldrich) for 1 hour at room temperature. Detection was performed using SuperSignal West Pico PLUS Chemiluminescent Substrate (Thermo Fisher Scientific).

For hemolymph samples, hemolymph was collected as previously described, and protein concentration was determined using Pierce™ BCA Protein Assay (Thermo Fisher). A total of 30 µg of hemolymph protein was mixed with reducing sample buffer, resolved on a NuPAGE™ 10% Bis-Tris Protein Gel, and transferred to a PVDF membrane as described above. Membranes were incubated overnight at 4°C with rabbit anti-CLIPA14 (Bio Booster, 1:500) and mouse anti-apyrase (1:500) in blocking buffer. Following three washes with PBST, detection was conducted using SuperSignal West Pico PLUS Chemiluminescent Substrate for CLIPA14 and SuperSignal™ West Atto Ultimate Sensitivity Substrate for apyrase. Imaging was performed with an iBright Imager (Thermo Fisher).

Real-time PCR

Pools of 20 pairs of SGs from uninfected or *P. berghei*-infected mosquitoes were collected into 200 µl of TRIzol™ reagent (77)(ThermoFisher,) and homogenized using a motorized pestle. The SG homogenates were processed with TRIzol LS according to the manufacturer's protocol for RNA extraction. After RNA precipitation with isopropanol, the RNA pellets were washed twice with 300 µl of 75% ethanol. The tubes were mixed by vortexing and centrifuged at 7500 RCF for 5 minutes at 4 °C. The RNA pellets were then solubilized in 21 µl of RNase-free water by gentle pipetting, followed by incubation at 55 °C for 10 minutes to fully

resuspend the RNA. All extracted RNA was used for complementary DNA (cDNA) synthesis using the QuantiTect Reverse Transcription Kit (Qiagen, Germantown, MD, USA) according to the manufacturer's instructions. Gene expression was assessed by quantitative PCR (qPCR) on a QuantStudio 7 real-time PCR system (Applied Biosystems). Semi-quantitative qPCR was used to measure the expression levels of the genes A5R1, Apy, AAPP, NT5E, D7R3, Tranf 1, LP, CLIPA14, and PPO6. Relative expression levels were normalized to *An. gambiae* ribosomal protein S7 (RpS7) as the internal control, and data analysis was conducted using the ΔΔ Ct method (78, 79). Statistical analysis of the fold change in gene expression was performed using an unpaired t-test (GraphPad, San Diego, CA, USA). Each experiment included at least three biological replicates per condition. The primers used for qPCR are listed in Table S1.

Data availability

All data needed to evaluate the conclusions are included in the paper, the Supplementary Materials have been deposited in online repositories. The mass spectrometry proteomics data have been deposited to the ProteomeXchange Consortium via the PRIDE partner repository with the dataset identifiers: PXD057628 (PXD057628), PXD057587 (Saliva), and PXD057585 (Hemolymph). Source data are provided with this paper.

Acknowledgements

The authors are grateful to Andre Laughinghouse and Kevin Lee for insectary support. We would like to thank Drs. Abhai Tripathi and Godfree Mlambo, and Chris Kizito the Insectary and Parsitology Core Facilities team at the Johns Hopkins Malaria Research Institute (JHMRI). We are grateful to Bloomberg Philanthropies for support of this facility and the work being performed at

JHMRI. **Funding:** This work was supported by the NIH Distinguished Scholars Program and the Intramural Research Program of the Division of Intramural Research (AI001250-01), National Institute of Allergy and Infectious Diseases (NIAID), NIH to JVR. This work was supported by a JHMRI fellowship to SK, the National Institutes of Health (R01AI132359 to PS and R03AI180804 to SK), and the Howard Hughes Medical Institute to PS and SK.

Author Contributions

Conceptualization: T.L.A.S., and J.V.R. Methodology: T.L.A.S., S.K., P.S., A.B.B.F, C.S., O.A.C.T, B.N., M.Z., M.S., L.P.D, I.C., C.B.M., and J.V.R.; Investigation: T.L.A.S., S.K., A.B.B.F., C.S., O.A.C.T., J.O., B.M.N., Z.R.P., T.P., D.A.A., M.Z., M.S., L.P.D., F.F, I.C., J.M.C.R., and J.V.R.; Formal analysis: T.L.A.S., and J.V.R.; Writing – original draft: T.L.A.S. and J.V.R.; Supervision: J.V.R.

Competing Interests

The authors declare no competing interest. All data are available in the manuscript or the supplementary materials.

References

1. WHO (2023) World malaria report 2023.
2. R. G. A. Feachem *et al.*, Malaria eradication within a generation: ambitious, achievable, and necessary. *Lancet* **394**, 1056-1112 (2019).
3. P. F. Pimenta, M. Touray, L. Miller, The journey of malaria sporozoites in the mosquito salivary gland. *J Eukaryot Microbiol* **41**, 608-624 (1994).
4. A. K. Ghosh, M. Jacobs-Lorena, Plasmodium sporozoite invasion of the mosquito salivary gland. *Curr Opin Microbiol* **12**, 394-400 (2009).
5. S. Kanatani, D. Stiffler, T. Bousema, G. Yenokyan, P. Sinnis, Revisiting the Plasmodium sporozoite inoculum and elucidating the efficiency with which malaria parasites progress through the mosquito. *Nat Commun* **15**, 748 (2024).
6. S. Briquet, C. Marinach, O. Silvie, C. Vaquero, Preparing for Transmission: Gene Regulation in Plasmodium Sporozoites. *Front Cell Infect Microbiol* **10**, 618430 (2020).
7. S. E. Lindner *et al.*, Transcriptomics and proteomics reveal two waves of translational repression during the maturation of malaria parasite sporozoites. *Nat Commun* **10**, 4964 (2019).
8. H. N. Bogale *et al.*, Transcriptional heterogeneity and tightly regulated changes in gene expression during Plasmodium berghei sporozoite development. *Proc Natl Acad Sci U S A* **118** (2021).
9. R. Pinheiro-Silva *et al.*, Gene expression changes in the salivary glands of Anopheles coluzzii elicited by Plasmodium berghei infection. *Parasit Vectors* **8**, 485 (2015).
10. G. Costa *et al.*, Non-competitive resource exploitation within mosquito shapes within-host malaria infectivity and virulence. *Nat Commun* **9**, 3474 (2018).
11. B. Arca, J. M. Ribeiro, Saliva of hematophagous insects: a multifaceted toolkit. *Curr Opin Insect Sci* **29**, 102-109 (2018).
12. D. S. Yamamoto, M. Sumitani, K. Kasashima, H. Sezutsu, H. Matsuoka, Inhibition of Malaria Infection in Transgenic Anopheline Mosquitoes Lacking Salivary Gland Cells. *PLoS Pathog* **12**, e1005872 (2016).
13. J. M. Ribeiro, P. A. Rossignol, A. Spielman, Role of mosquito saliva in blood vessel location. *J Exp Biol* **108**, 1-7 (1984).
14. T. R. Schleicher *et al.*, A mosquito salivary gland protein partially inhibits Plasmodium sporozoite cell traversal and transmission. *Nat Commun* **9**, 2908 (2018).
15. Y. M. Chuang *et al.*, The Effects of A Mosquito Salivary Protein on Sporozoite Traversal of Host Cells. *J Infect Dis* **224**, 544-553 (2021).
16. P. A. Rossignol, J. M. Ribeiro, A. Spielman, Increased intradermal probing time in sporozoite-infected mosquitoes. *Am J Trop Med Hyg* **33**, 17-20 (1984).
17. D. E. Kalume *et al.*, A proteomic analysis of salivary glands of female mosquito. *Proteomics* **5**, 3765-3777 (2005).
18. V. Choumet *et al.*, The salivary glands and saliva of as an essential step in the Plasmodium life cycle:: A global proteomic study. *Proteomics* **7**, 3384-3394 (2007).
19. J. C. Koella, F. L. Sorensen, R. A. Anderson, The malaria parasite, Plasmodium falciparum, increases the frequency of multiple feeding of its mosquito vector, Anopheles gambiae. *Proc Biol Sci* **265**, 763-768 (1998).
20. K. Thievent, G. Zilio, G. Hauser, J. C. Koella, Malaria load affects the activity of mosquito salivary apyrase. *J Insect Physiol* **116**, 10-16 (2019).

21. M. Hajkazemian *et al.*, Mosquito host-seeking diel rhythm and chemosensory gene expression is affected by age and Plasmodium stages. *Sci Rep* **12**, 18814 (2022).
22. P. A. Rossignol, J. M. Ribeiro, A. Spielman, Increased biting rate and reduced fertility in sporozoite-infected mosquitoes. *Am J Trop Med Hyg* **35**, 277-279 (1986).
23. X. Li, B. Sina, P. A. Rossignol, Probing behaviour and sporozoite delivery by Anopheles stephensi infected with Plasmodium berghei. *Med Vet Entomol* **6**, 57-61 (1992).
24. M. B. Wells, D. J. Andrew, Anopheles Salivary Gland Architecture Shapes Plasmodium Sporozoite Availability for Transmission. *mBio* **10** (2019).
25. J. F. Krey *et al.*, Mass spectrometry quantitation of proteins from small pools of developing auditory and vestibular cells. *Sci Data* **5**, 180128 (2018).
26. B. Schwanhausser *et al.*, Corrigendum: Global quantification of mammalian gene expression control. *Nature* **495**, 126-127 (2013).
27. H. Nielsen, J. Engelbrecht, S. Brunak, G. von Heijne, Identification of prokaryotic and eukaryotic signal peptides and prediction of their cleavage sites. *Protein Eng* **10**, 1-6 (1997).
28. E. Masini *et al.*, The role of histamine in platelet aggregation by physiological and immunological stimuli. *Inflamm Res* **47**, 211-220 (1998).
29. L. B. Smith *et al.*, Novel salivary antihemostatic activities of long-form D7 proteins from the malaria vector Anopheles gambiae facilitate hematophagy. *J Biol Chem* **298**, 101971 (2022).
30. H. A. Johnston-Cox, K. Ravid, Adenosine and blood platelets. *Purinergic Signal* **7**, 357-365 (2011).
31. R. M. Berne, R. M. Knabb, S. W. Ely, R. Rubio, Adenosine in the local regulation of blood flow: a brief overview. *Fed Proc* **42**, 3136-3142 (1983).
32. G. Magni, S. Ceruti, Adenosine Signaling in Autoimmune Disorders. *Pharmaceuticals (Basel)* **13** (2020).
33. I. A. Droujinine *et al.*, Proteomics of protein trafficking by in vivo tissue-specific labeling. *Nat Commun* **12**, 2382 (2021).
34. X. Sun, J. Shen, N. Perrimon, X. Kong, D. Wang, The endoribonuclease Arlr is required to maintain lipid homeostasis by downregulating lipolytic genes during aging. *Nat Commun* **14**, 6254 (2023).
35. G. C. Atella, P. R. Bittencourt-Cunha, R. D. Nunes, M. Shahabuddin, M. A. Silva-Neto, The major insect lipoprotein is a lipid source to mosquito stages of malaria parasite. *Acta Trop* **109**, 159-162 (2009).
36. S. Herzig *et al.*, Identification and functional expression of the mitochondrial pyruvate carrier. *Science* **337**, 93-96 (2012).
37. D. K. Bricker *et al.*, A mitochondrial pyruvate carrier required for pyruvate uptake in yeast, Drosophila, and humans. *Science* **337**, 96-100 (2012).
38. S. A. Watson, G. P. McStay, Functions of Cytochrome c oxidase Assembly Factors. *Int J Mol Sci* **21** (2020).
39. C. C. Murdoch, E. P. Skaar, Nutritional immunity: the battle for nutrient metals at the host-pathogen interface. *Nat Rev Microbiol* **20**, 657-670 (2022).
40. I. Iatsenko, A. Marra, J. P. Boquete, J. Pena, B. Lemaitre, Iron sequestration by transferrin 1 mediates nutritional immunity in Drosophila melanogaster. *Proc Natl Acad Sci U S A* **117**, 7317-7325 (2020).
41. M. Povelones, R. M. Waterhouse, F. C. Kafatos, G. K. Christophides, Leucine-rich repeat protein complex activates mosquito complement in defense against Plasmodium parasites. *Science* **324**, 258-261 (2009).
42. M. Fraiture *et al.*, Two mosquito LRR proteins function as complement control factors in the TEP1-mediated killing of Plasmodium. *Cell Host Microbe* **5**, 273-284 (2009).

43. J. Volz, H. M. Muller, A. Zdanowicz, F. C. Kafatos, M. A. Osta, A genetic module regulates the melanization response of Anopheles to Plasmodium. *Cell Microbiol* **8**, 1392-1405 (2006).
44. R. Zakhia, M. A. Osta, CLIPA7 Exhibits Pleiotropic Roles in the Anopheles gambiae Immune Response. *J Innate Immun* **15**, 1-16 (2022).
45. H. Kwon, R. C. Smith, Chemical depletion of phagocytic immune cells in Anopheles gambiae reveals dual roles of mosquito hemocytes in anti-Plasmodium immunity. *Proc Natl Acad Sci U S A* **116**, 14119-14128 (2019).
46. J. K. Johnson *et al.*, A potential role for phenylalanine hydroxylase in mosquito immune responses. *Insect Biochem Mol Biol* **33**, 345-354 (2003).
47. L. C. Infanger *et al.*, The role of phenylalanine hydroxylase in melanotic encapsulation of filarial worms in two species of mosquitoes. *Insect Biochem Mol Biol* **34**, 1329-1338 (2004).
48. M. Y. Noh, S. Mun, K. J. Kramer, S. Muthukrishnan, Y. Arakane, Yellow-y Functions in Egg Melanization and Chorion Morphology of the Asian Tiger Mosquito, Aedes albopictus. *Front Cell Dev Biol* **9**, 769788 (2021).
49. S. K. Kolli *et al.*, Malaria parasite evades mosquito immunity by glutaminyl cyclase-mediated posttranslational protein modification. *Proc Natl Acad Sci U S A* **119**, e2209729119 (2022).
50. R. H. N. José M. C. Ribeiro, The Salivary Catechol Oxidase/Peroxidase Activities of the Mosquito Anopheles Albimanus. *Journal of Experimental Biology* **179**, 273-287 (1993).
51. J. M. Ribeiro, R. H. Nussenzveig, G. Tortorella, Salivary vasodilators of Aedes triseriatus and Anopheles gambiae (Diptera: Culicidae). *J Med Entomol* **31**, 747-753 (1994).
52. J. M. Ribeiro, J. G. Valenzuela, Purification and cloning of the salivary peroxidase/catechol oxidase of the mosquito Anopheles albimanus. *J Exp Biol* **202**, 809-816 (1999).
53. T. Dottorini *et al.*, A genome-wide analysis in Anopheles gambiae mosquitoes reveals 46 male accessory gland genes, possible modulators of female behavior. *Proc Natl Acad Sci U S A* **104**, 16215-16220 (2007).
54. S. M. Paskewitz, L. Shi, The hemolymph proteome of Anopheles gambiae. *Insect Biochem Mol Biol* **35**, 815-824 (2005).
55. Z. Zou *et al.*, Mosquito RUNX4 in the immune regulation of PPO gene expression and its effect on avian malaria parasite infection. *Proc Natl Acad Sci U S A* **105**, 18454-18459 (2008).
56. C. Karlsson *et al.*, Proteomic analysis of the Drosophila larval hemolymph clot. *J Biol Chem* **279**, 52033-52041 (2004).
57. O. Marinotti, L. Capurro Mde, X. Nirmala, E. Calvo, A. A. James, Structure and expression of the lipophorin-encoding gene of the malaria vector, Anopheles gambiae. *Comp Biochem Physiol B Biochem Mol Biol* **144**, 101-109 (2006).
58. G. Raddi *et al.*, Mosquito cellular immunity at single-cell resolution. *Science* **369**, 1128-1132 (2020).
59. H. Kwon, M. Mohammed, O. Franzen, J. Ankarklev, R. C. Smith, Single-cell analysis of mosquito hemocytes identifies signatures of immune cell subtypes and cell differentiation. *Elife* **10** (2021).
60. P. Fernandes *et al.*, The AMA1-RON complex drives Plasmodium sporozoite invasion in the mosquito and mammalian hosts. *PLoS Pathog* **18**, e1010643 (2022).
61. G. Arora, Y. M. Chuang, P. Sinnis, G. Dimopoulos, E. Fikrig, Malaria: influence of Anopheles mosquito saliva on Plasmodium infection. *Trends Immunol* **44**, 256-265 (2023).

62. V. Choumet *et al.*, The salivary glands and saliva of Anopheles gambiae as an essential step in the Plasmodium life cycle: a global proteomic study. *Proteomics* **7**, 3384-3394 (2007).
63. V. O. Nyasembe *et al.*, Adipokinetic hormone signaling in the malaria vector Anopheles gambiae facilitates Plasmodium falciparum sporogony. *Commun Biol* **6**, 171 (2023).
64. T. Yoshiga, V. P. Hernandez, A. M. Fallon, J. H. Law, Mosquito transferrin, an acute-phase protein that is up-regulated upon infection. *Proc Natl Acad Sci U S A* **94**, 12337-12342 (1997).
65. N. Trisnadi, C. Barillas-Mury, Live In Vivo Imaging of Plasmodium Invasion of the Mosquito Midgut. *mSphere* **5** (2020).
66. A. Ayyaz, H. Li, H. Jasper, Haemocytes control stem cell activity in the Drosophila intestine. *Nat Cell Biol* **17**, 736-748 (2015).
67. Y. Yu *et al.*, Macrophages play a key role in tissue repair and regeneration. *PeerJ* **10**, e14053 (2022).
68. J. Nakhleh, G. K. Christophides, M. A. Osta, The serine protease homolog CLIPA14 modulates the intensity of the immune response in the mosquito Anopheles gambiae. *J Biol Chem* 10.1074/jbc.M117.797787 (2017).
69. S. Zeineddine *et al.*, Late sporogonic stages of Plasmodium parasites are susceptible to the melanization response in Anopheles gambiae mosquitoes. *bioRxiv* 10.1101/2024.05.31.596773 (2024).
70. Z. R. Pala *et al.*, Anopheles salivary apyrase regulates blood meal hemostasis and drives malaria parasite transmission. *bioRxiv* 10.1101/2023.05.22.541827 (2023).
71. D. Klug, A. Gautier, E. Calvo, E. Marois, S. A. Blandin, The salivary protein Saglin facilitates efficient midgut colonization of Anopheles mosquitoes by malaria parasites. *PLoS Pathog* **19**, e1010538 (2023).
72. H. Hurd, P. J. Taylor, D. Adams, A. Underhill, P. Eggleston, Evaluating the costs of mosquito resistance to malaria parasites. *Evolution* **59**, 2560-2572 (2005).
73. M. Prado *et al.*, Long-term live imaging reveals cytosolic immune responses of host hepatocytes against Plasmodium infection and parasite escape mechanisms. *Autophagy* **11**, 1561-1579 (2015).
74. A. K. Tripathi, G. Mlambo, S. Kanatani, P. Sinnis, G. Dimopoulos, Plasmodium falciparum Gametocyte Culture and Mosquito Infection Through Artificial Membrane Feeding. *J Vis Exp* 10.3791/61426 (2020).
75. S. Tyanova *et al.*, The Perseus computational platform for comprehensive analysis of (prote)omics data. *Nat Methods* **13**, 731-740 (2016).
76. J. F. Krey *et al.*, Accurate label-free protein quantitation with high- and low-resolution mass spectrometers. *J Proteome Res* **13**, 1034-1044 (2014).
77. J. W. Cheng, Tezosentan in the management of decompensated heart failure. *Cardiol Rev* **13**, 28-34 (2005).
78. K. J. Livak, T. D. Schmittgen, Analysis of relative gene expression data using real-time quantitative PCR and the 2(-Delta Delta C(T)) Method. *Methods* **25**, 402-408 (2001).
79. M. W. Pfaffl, A new mathematical model for relative quantification in real-time RT-PCR. *Nucleic Acids Res* **29**, e45 (2001).

Figures

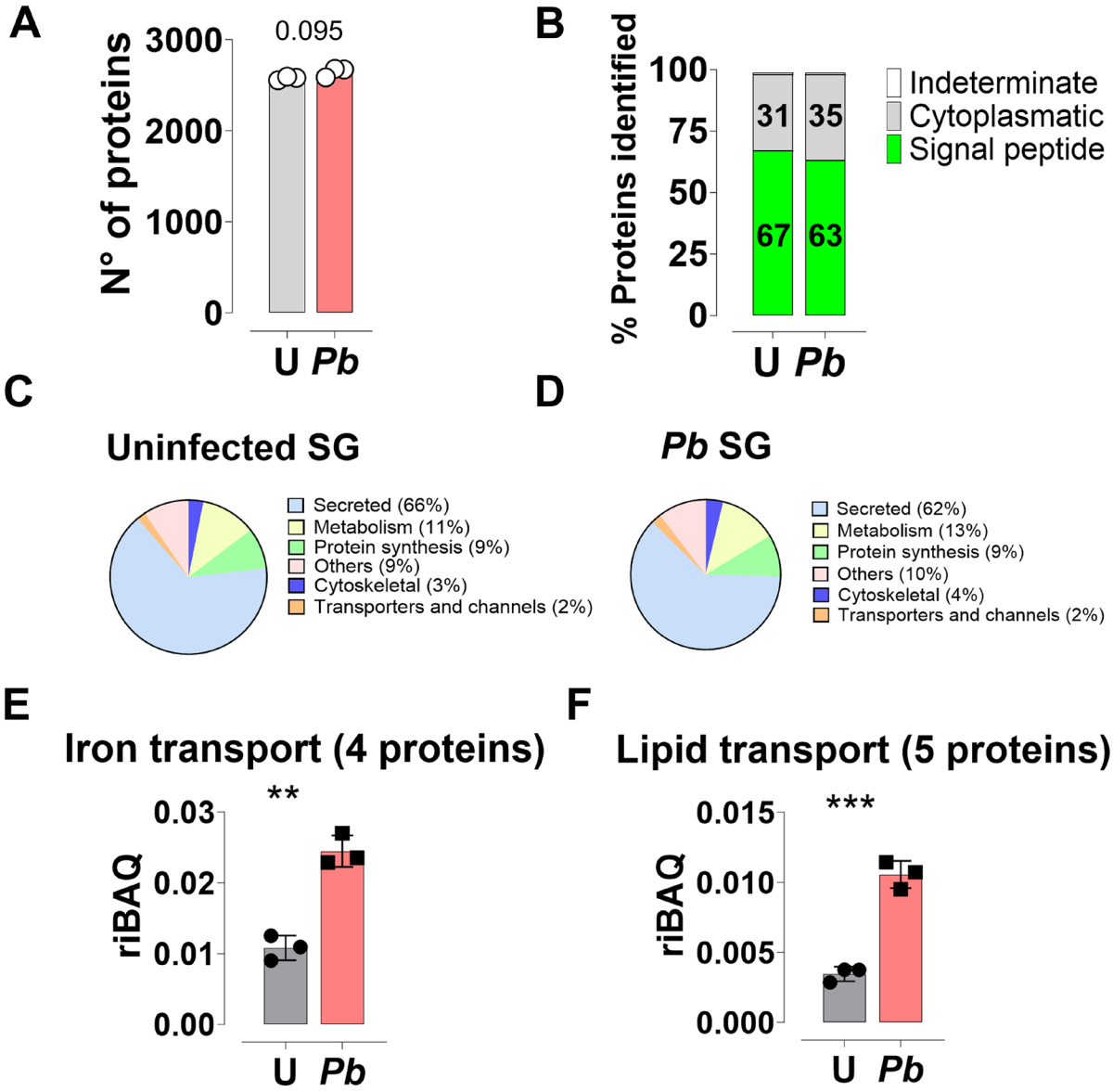

Figure 1. Proteomic analysis of uSGs (U) and *P. berghei*-iSGs (*Pb*). (A) Total proteins identified using MaxLFQ in uSGs and iSGs. Analyses were conducted on three independent pools (N = 3), each containing 25 pairs of SGs. No significant difference was found using the t-test (P = 0095). (B) The classification of proteins predicted by SignalP 5.0 is shown as a percentage relative to iBAQ. Numbers inside the bar represent the percentage of each category. (C-D) Relative protein

abundance of functional classes in the salivary gland proteome of uninfected (C) and infected (D) mosquitoes, expressed as a percentage based on iBAQ values. (E-F) Relative abundance of iron (E) and lipid (F) transport proteins in uSGs and iSGs. The number of proteins identified in each category is indicated in parentheses. Data represent the mean values from three independent experiments ± standard deviation of the mean (SD). Statistical significance was determined using the Student's t-test (**P < 0.01, ***P < 0.001).

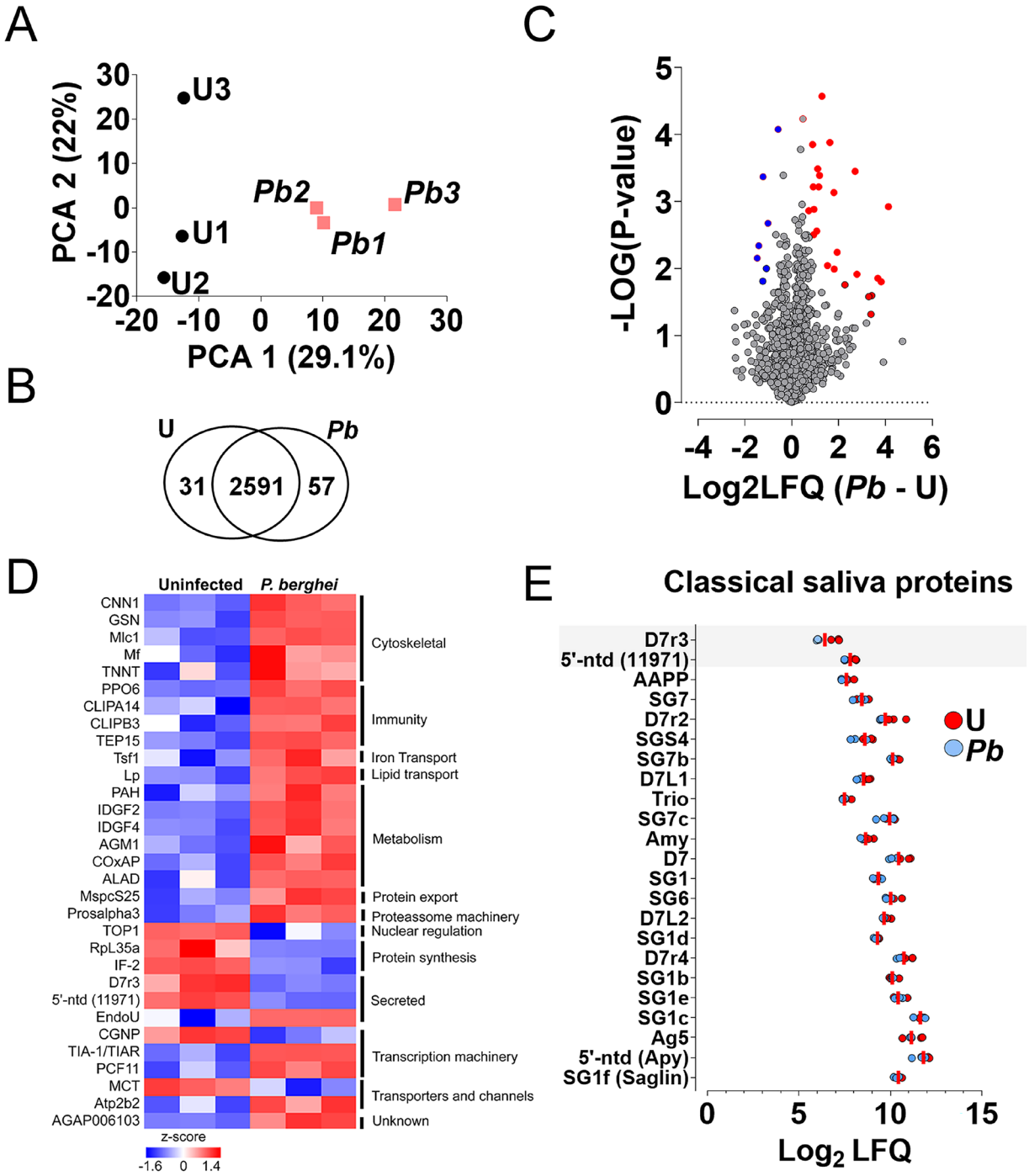

Figure 2. Differential protein expression in uninfected (U) and *P. berghei*-iSGs (*Pb*). (A) Principal component analysis (PCA) of normalized protein abundances based on MaxLFQ values for uSGs and *Pb* iSGs. Colors represent different experimental conditions, and labels identify individual samples. (B) Venn diagram

showing the total number of proteins identified in independent samples. (n=3) (C) Volcano plot of differential protein expression between uSGs and iSGs. The x-axis represents $\log_2$ fold changes, while the y-axis shows significance ($-\log_{10}$ p-value). Proteins downregulated in iSGs are marked in blue, and proteins upregulated are marked in red. Only proteins detected in both conditions are included. (D) Heatmap of 21 differentially expressed proteins between uSGs and *Pb* iSGs samples. Protein expression values were Z-transformed and normalized across conditions. Rows (individual proteins) are ordered by function and clustered using Euclidean distance. (E) Dot plot showing the abundance of classical saliva proteins in uSGs and iSGs. Each dot represents the Log_2 LFQ values for individual proteins in uSGs (red) and iSGs (blue). Proteins are listed on the vertical axis, and Log_2 LFQ values on the horizontal axis indicate relative abundance. The shadowed areas indicate abundant proteins differentially expressed.

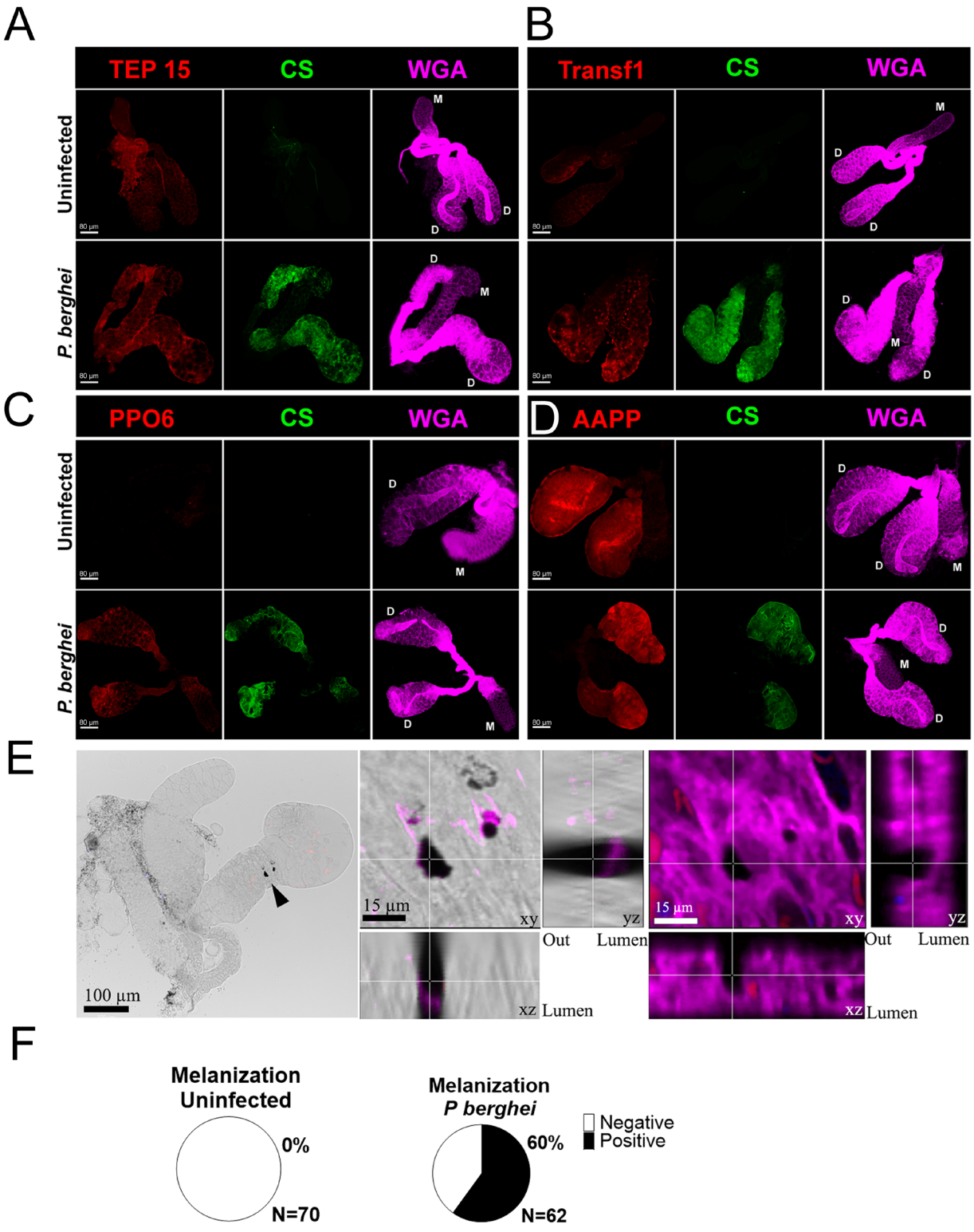

Figure 3. Detection of differentially expressed salivary gland proteins. SGs were stained for different proteins and visualized using confocal microscopy. (A)

Thioester-containing protein 15 (TEP 15), (B) Transferrin 1 (Transf1), (C) Prophenoloxidase 6 (PPO6), and (D) *Anopheles* antiplatelet protein (AAPP). Additionally, *P. berghei* circumsporozoite protein (CS) and wheat germ agglutinin (WGA) were used to visualize infected tissues and SG cell surface, respectively. D: distal lobes, M: medial lobe. Scale bar (A-D) 80 µm. (E) Melanization in salivary glands. Bright-field imaging (panel 1) displays the whole salivary gland. Panel 2 shows sections of the salivary glands, with the white line indicating the focal plane of the images. Panel 3 shows fluorescence images of panel 2, WGA staining in magenta, marking the surface of the salivary gland; sporozoites, stained with mCherry in red; cell nuclei, stained with Hoechst, are shown in blue. (F) Prevalence of melanization spots in uninfected and iSGs.

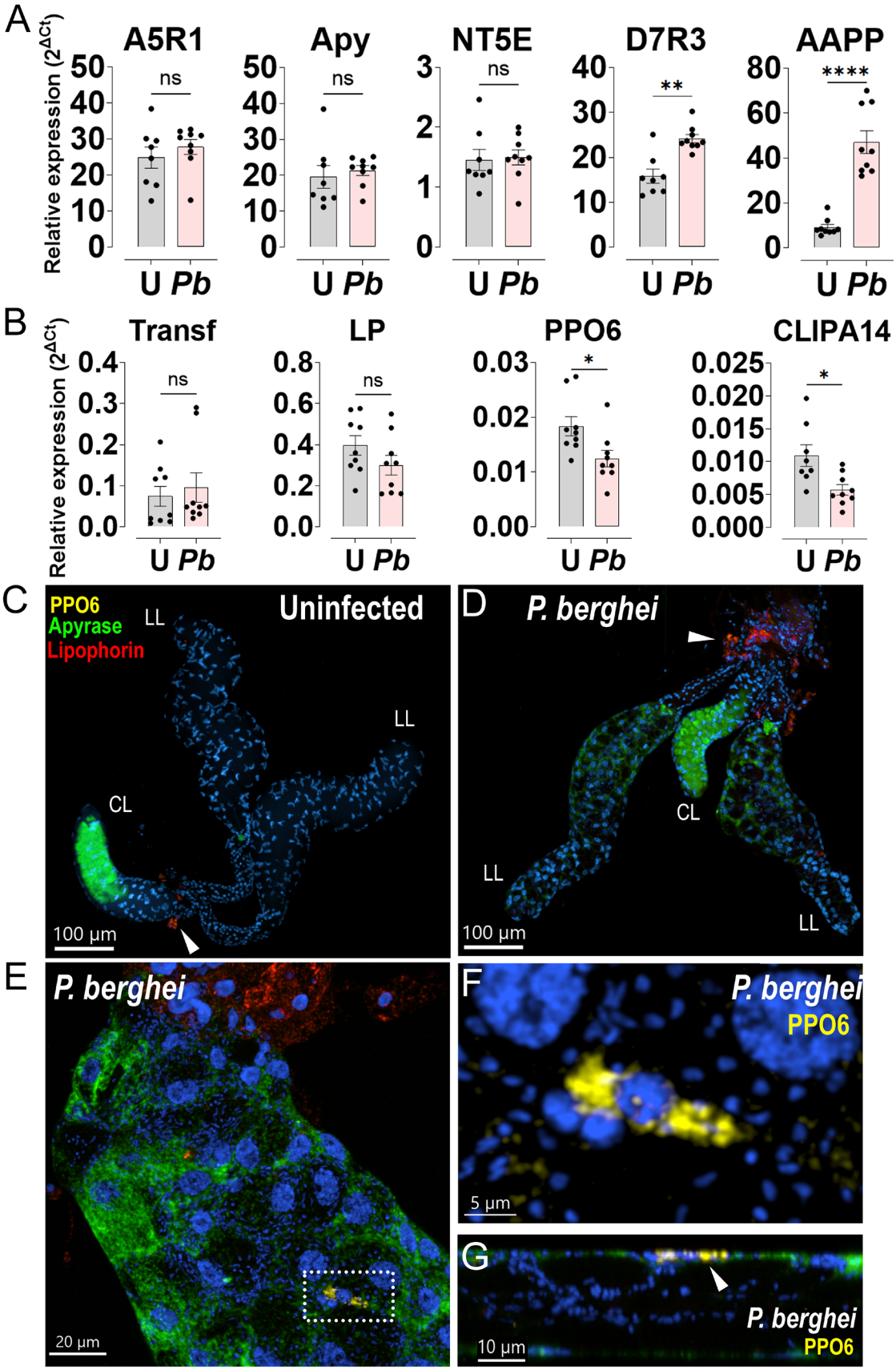

Figure 4. Transcriptional activity in uSGs (U) and *P. berghei*-iSGs (*Pb*). (A) Relative mRNA expression of selected classical saliva genes by qRT-PCR analyses in uSGs and iSGs 20 days post-infection. Antigen 5-related protein 1 (A5R1), apyrase (Apy), *Anopheles* antiplatelet protein (AAPP), 5'nucleotidase ecto (NT5E), D7-related protein 3 (D7R3). Relative expression levels were calculated using the delta-delta Ct (ΔΔCt) method, with ribosomal protein S7 used as the reference gene for normalization. (B) Selected proteins showing differential expression between uSGs and iSGs. Transferrin 1 (Transf), lipophorin (LP), clip domain serine protease related protein A 14 (CLIPA14) and prophenoloxidase 6 (PPO6). Bars: Mean fold change in gene expression relative to uninfected controls ± SD. Dots: Individual biological replicates. Differences in relative expression between the conditions were determined using an unpaired t-test (Mann-Whitney). Significance levels are indicated as: *P ≤ 0.05, **P ≤ 0.01, ***P ≤ 0.001, ****P ≤ 0.0001. (C) . RNA in situ hybridization in uSGs (C) and (D) iSGs. Nuclei in blue, PPO6 in yellow, Apyrase in green and Lipophorin in red. (LL) lateral lobe and (CL) central lobe. Arrow in (C) and (D) indicates fat body cells associated with SGs. (E) Close-up of an iSG. Nuclei in blue, PPO6 in yellow, Apyrase in green and Lipophorin in red. Dashed insert identifies a PPO6-positive hemocyte in the surface of an iSGs. (F) Close-up of a PPO6-positive hemocyte. (G) Lateral view of an iSG with a hemocyte expressing PPO6 RNA. Arrow indicates hemocyte in the surface of the lobe.

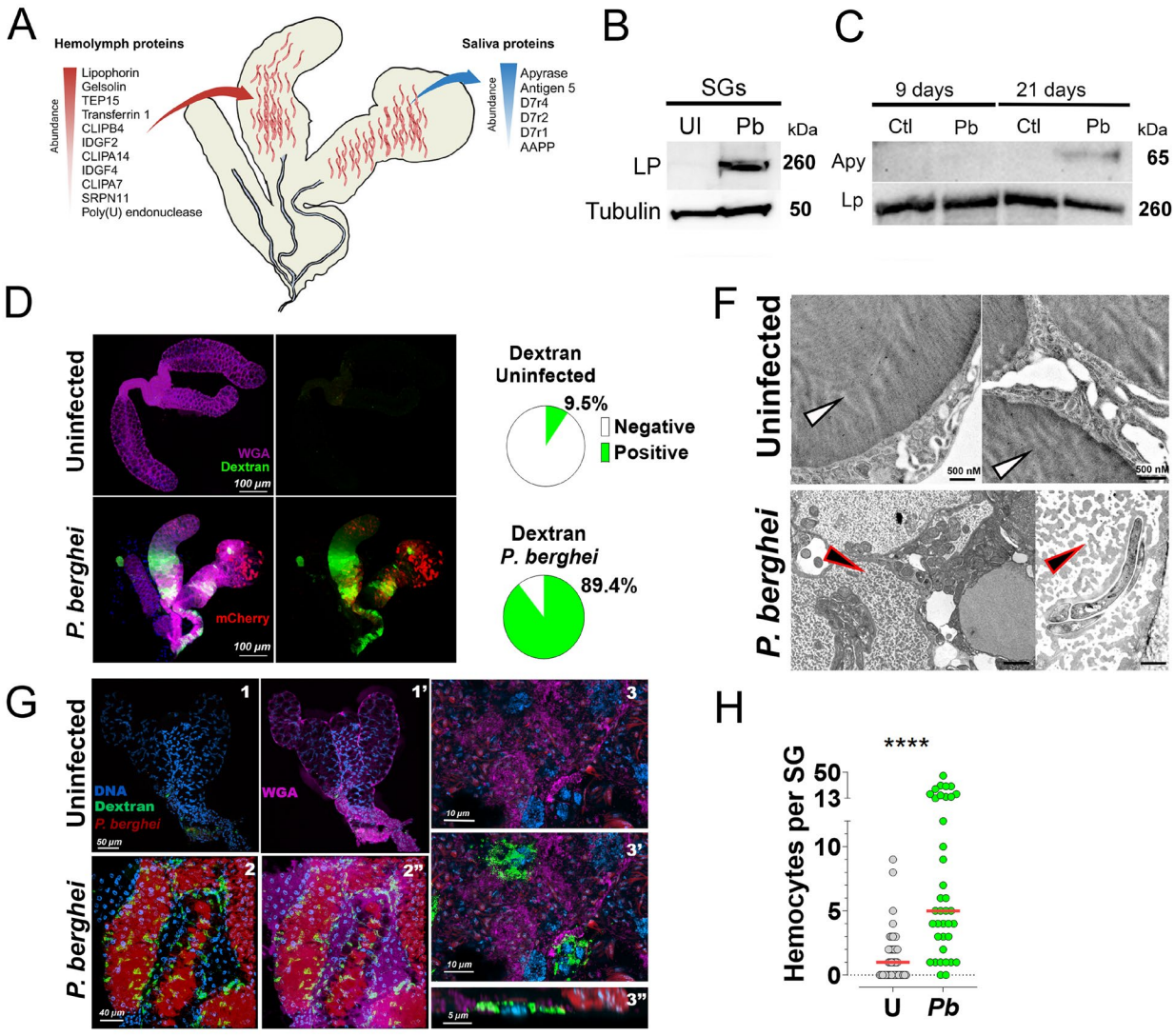

Figure 5. Analysis of epithelial integrity in SGs. (A) Diffusion of proteins into and out of salivary glands. Listed on the left are the most abundant hemolymph proteins enriched within the salivary glands. On the right, the saliva proteins exclusively found in the infected hemolymph at 19 days post-infection. The arrows represent the direction of protein diffusion. (B) Western blot analysis of lipophorin (LP) expression in uSGs (UI) and iSGs (Pb) at 21 days post-infection. Tubulin used as a loading control. (C) Western blot analysis of apyrase expression in (UI) and iSGs at 9 and 21 days post-infection. No SG invasion is detected at 9 days; however, SGs are heavily infected by 21 days. Lipophorin is used as a loading

control. (D) Dextran diffusion assay: Fluorescent dextran (10 kDa) diffusion in uSGs and iSGs 21 days post-infection. Images display green fluorescent dextran, red mCherry parasites, and magenta WGA staining. (E) Pie charts summarize dextran diffusion quantification from two independent experiments. Chi-square statistic = 51.1359; $p < 0.00001$. (F) *P. berghei* infection of salivary glands changes the texture of saliva within the secretory cavities. (F) Representative images of salivary glands (SGs) from *An. gambiae*, either uninfected or infected with *P. berghei*. Note the electro-lucent areas and granular texture in the saliva of infected SGs (black arrow), suggesting saliva protein loss, and the homogeneous texture of saliva in uninfected SGs (white arrow). (G) Interaction of hemocytes with SGs. Fluorescence images showing interactions between hemocytes with uSGs and iSGs. Staining includes DNA (blue), dextran (green), mCherry (red), and WGA (magenta). Uninfected glands: 1 and 1', infected glands: 2 to 3''. WGA was omitted in 1 and 2. Merged colors: 1' and 2'. Closer view of iSGs: 3, 3'. Lateral view of iSGs: 3''. (H) Quantification of hemocyotes bound to the SGs. Dot plot showing the number of hemocytes associated with uSGs (U) and iSGs (I). The graph represents two independent experiments. Differences in relative expression between the conditions were determined using Mann-Whitney. The horizontal red line represents the median. Significance levels are indicated as ****$P \leq 0.0001$.

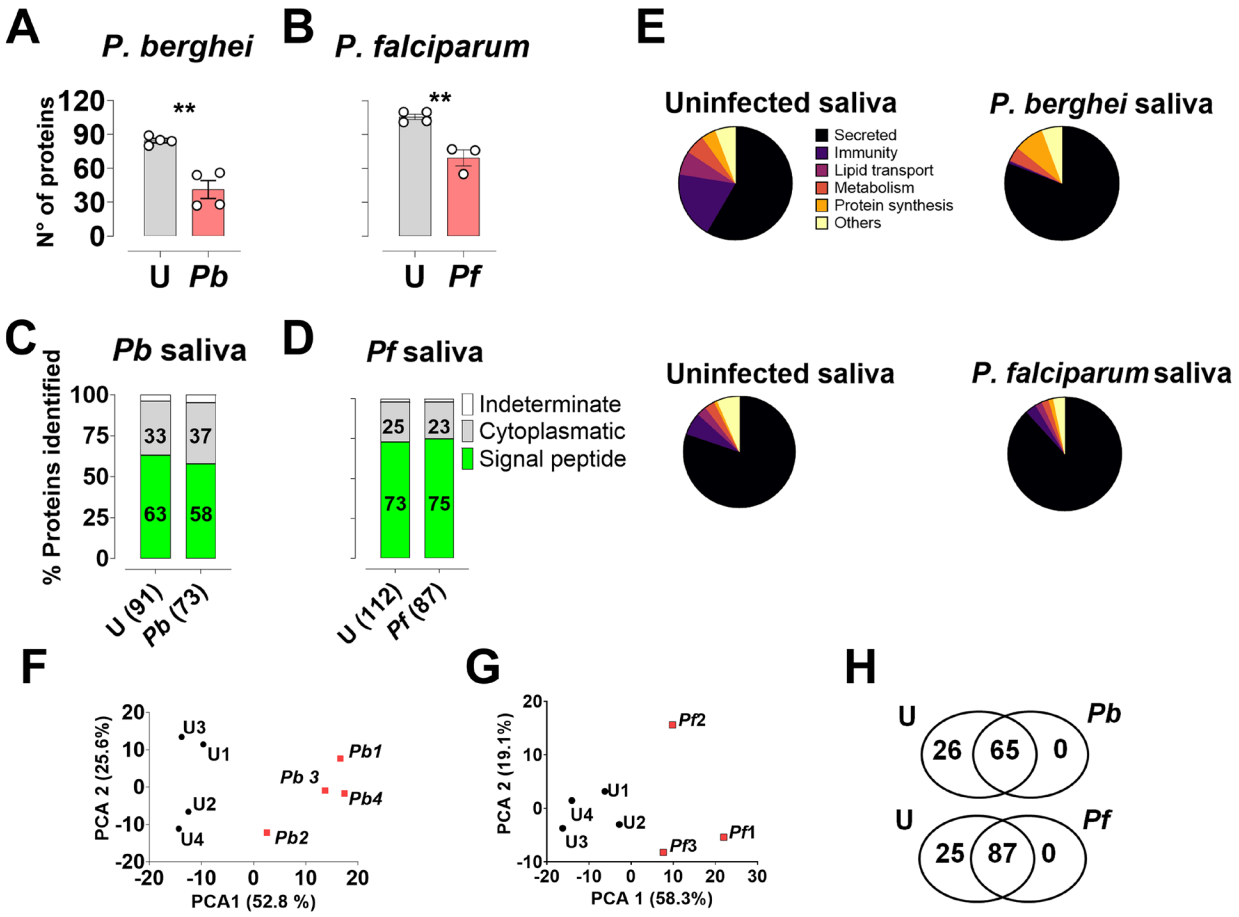

Figure 6: Proteomic analysis of uninfected (U), *P. berghei* (Pb)- and *P. falciparum*-infected saliva (Pf). A-B. Total proteins identified using MaxLFQ in the saliva of *P. berghei* (A) and *P. falciparum* (B) infected mosquitoes. Analyses were conducted on four independent pools (t-test, **P ≤ 0.01). (C-D) Classification of proteins predicted by SignalP 5.0, shown as percentage relative iBAQ. (E) Relative protein abundance of functional classes in the saliva proteome of uninfected and infected mosquitoes, expressed as a percentage based on iBAQ values. (F and G) Principal component analysis (PCA) of normalized protein abundances based on MaxLFQ values for uninfected and infected saliva. Different colors represent different experimental conditions, and labels identify individual samples. (H) Venn diagram of protein identification. The total number of proteins identified in independent samples (n=4) is plotted as a Venn diagram, showing

unique and common proteins between uninfected and infected conditions for each parasite.

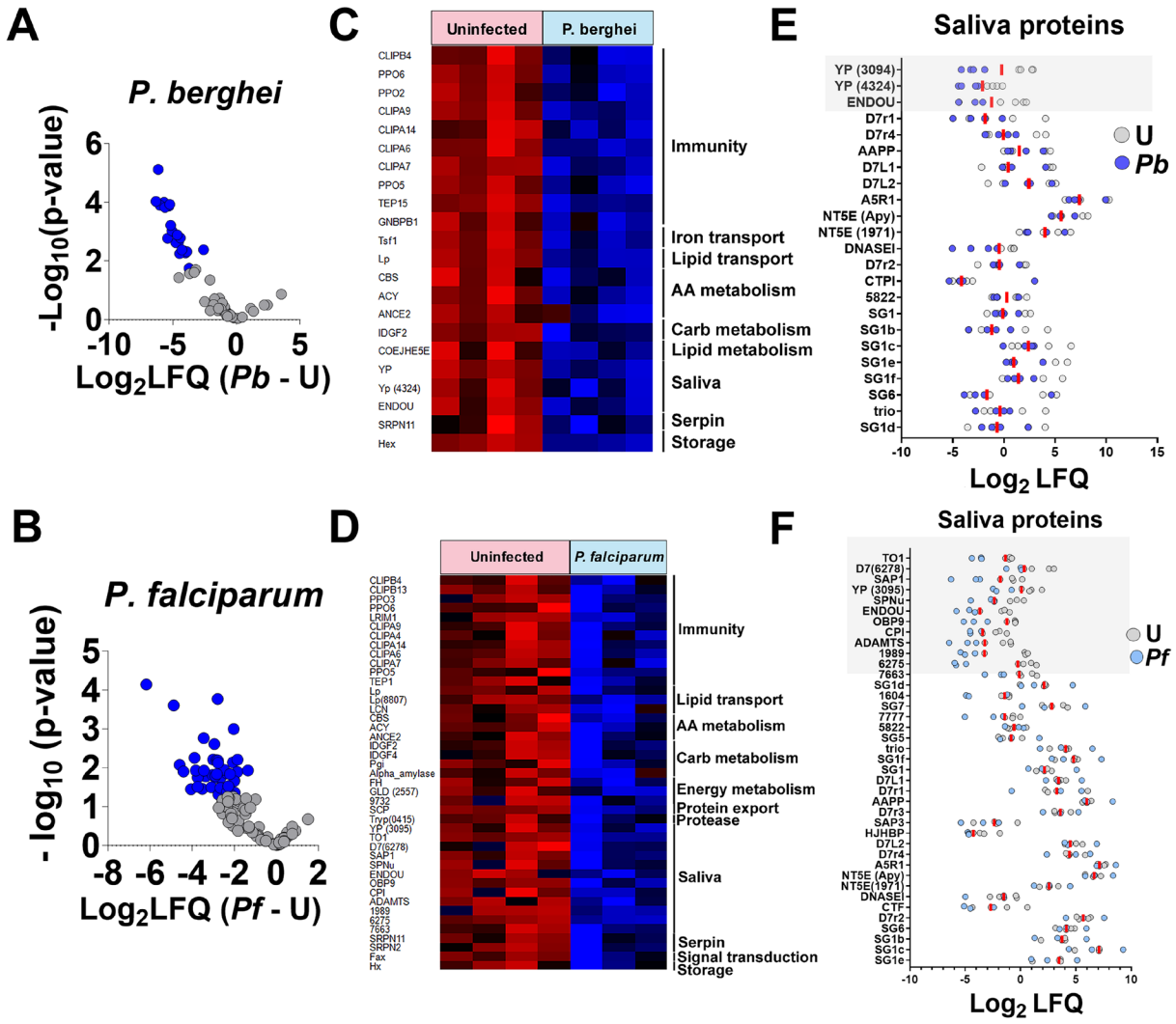

Figure 7. Differential protein enrichment or depletion in uninfected and *P. berghei*- or *P. falciparum*-infected saliva. (A and B) Volcano Plot of differential protein expression between uninfected (U) and *P. berghei*-infected saliva (*Pb*) (A) and uninfected and *P. falciparum*-infected saliva (B). The x-axis represents $\log_2$ fold changes, while the y-axis shows significance ($-\log_{10}$ p-value). Proteins depleted in infected saliva are marked in blue, and proteins enriched are marked in red. Only proteins detected in both conditions are included. (C and D) Heatmap of

differentially expressed proteins between uninfected and *P. berghei*-infected (C), and uninfected and *P. falciparum*-infected saliva (D). Protein expression values were Z-transformed and normalized across conditions. Rows (proteins) are ordered by function and clustered using Euclidean distance. (E and F) Dot plot showing the abundance of classical saliva proteins in uninfected and *P. berghei*-€ and uninfected and *P. falciparum*-infected mosquitoes (F). Each dot represents Log_2 LFQ values for individual proteins under uninfected (gray) and infected (blue) conditions. Proteins are listed on the vertical axis, and Log_2 LFQ values on the horizontal axis indicate relative abundance. The shadowed areas indicate abundant proteins differentially expressed.

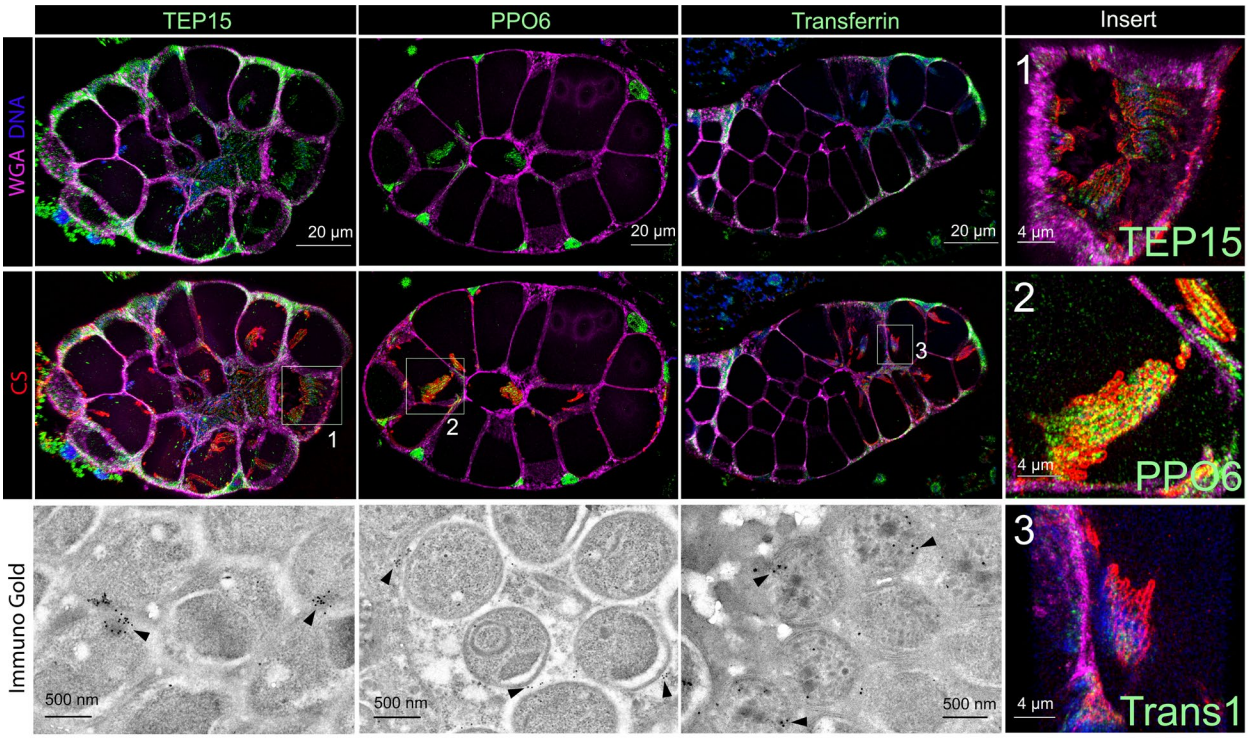

Figure 8: Histological immunofluorescence and immuno-transmission electron microscopy of uninfected and *P. berghei*-iSGs. These images display the distribution and association of immune proteins with the surface of *P. berghei* parasites in the SGs. Staining includes TEP15, PPO6, transferrin, AAPP (green),

circumsporozoite (red), and WGA (magenta). Note that AAPP shows a more diffuse distribution. Insert provides a closer view of stained *P. berghei* parasites, highlighting the spatial relationship between immune proteins and the parasite surface. Bottom images: immuno-TEM images showing the detailed interaction between immune proteins and *P. berghei* parasites — arrowheads showing immunogold staining of proteins, emphasizing the close association of immune proteins with the parasite surface.